Large-scale functional connectivity in multisensory cortex predicts performance

Karl J. Hollensteiner[1], Edgar Galindo-Leon[1], Florian Pieper[1], Gerhard Engler[1], Guido Nolte[1], Andreas K. Engel[1]

[1] Department of Neurophysiology and Pathophysiology, University Medical Center Hamburg-Eppendorf, 20246 Hamburg, Germany

Correspondence should be addressed to:
Karl J. Hollensteiner, Department of Neurophysiology and Pathophysiology, University Medical Center Hamburg-Eppendorf, 20246 Hamburg, Germany. Email: k.hollensteiner@uke.de

Abbreviated title: Functional connectivity in multisensory cortex predicts performance

Key words: ferret, electrocorticogram, functional connectivity, phase coupling, phase locking value, multisensory processing, auditory cortex, visual cortex

Number of figures: 7

Number of words: Abstract (150), Introduction (713), Results (2191), Discussion (3018), Materials and Methods (1614).

Abstract

Complex behavior requires fast changes of functional connectivity in large-scale cortical networks. Here, we report on the dynamics of functional coupling across visual, auditory and parietal areas during a lateralized detection task in the ferret. We hypothesized that fluctuations in coupling, indicative of dynamic variations in the network state, should be predictive of the animals' performance. Analysis of power for hit and miss trials revealed significant differences around stimulus- and response-onset. In contrast, phase coupling already differed between hits and misses before stimulus onset, indicating fluctuations in large-scale network connectivity. In particular, higher phase coupling of visual and auditory regions to parietal cortex was predictive of task performance. Furthermore, we observed that long-range coupling became more predominant during the task period compared to the pre-stimulus baseline. Taken together, these results suggest that fluctuations in the network state, particular with respect to long-range connectivity, are critical determinants of the animals' behavior.

Introduction

The brain continuously integrates information from different sensory systems enhancing its ability to detect noisy signals, to construct coherent percepts and guide appropriate actions (Stein and Meredith, 1993; Alais et al., 2010; Green and Angelaki, 2010; van Atteveldt et al., 2014). Such processes require the flexible orchestration of distributed neuronal populations within and across brain areas (Singer and Gray, 1995; Engel et al., 2001; Fries, 2005; Senkowski et al., 2008; Siegel et al., 2012). It has been proposed that coordination of distributed neural signals relies on several modes of intrinsically generated coupling which can involve synchronization of neural phase, correlation of amplitude envelopes, or phase-amplitude interactions (Raichle, 2010; Canolty and Knight, 2010; Siegel et al., 2012; Engel et al., 2013). Numerous studies have suggested that dynamic neuronal coupling operates in multiple frequency bands, which seem to be involved in mediating different cognitive functions (Fries, 2005; Buzsaki, 2006; Engel and Fries, 2010; Jensen and Mazaheri, 2010) or provide different channels for long-range communication (Bastos et al., 2015; Michalareas et al., 2016).

While substantial advances have been made in recent years in the analysis of dynamic functional connectivity in data recorded with non-invasive methods such as EEG or MEG (Brookes et al., 2011a; Siegel et al., 2012; Engel et al., 2013), a more mechanistic understanding requires the study of multi-site communication by direct recordings from the neural substrate. Approaches for invasive measurements of dynamic neural interactions are well established at the level of microcircuits (Coulter et al., 2011; Bastos et al., 2012; Feldmeyer et al., 2013), but addressing large-scale functional connectivity in relation to task performance or cognitive processing has remained a challenge. Invasive studies that addressed functional connectivity between distant population in behaving animals typically have recorded simultaneously only from relatively small numbers of sites. This holds, e.g., for studies of the coupling between early and higher-order visual cortex, or visual and prefrontal cortex subserving attentional selection (Womelsdorf and Fries, 2007; Gregoriou et al., 2009; Miller and Buschman, 2013) or of coupling between frontal and parietal-occipital regions during working memory (Liebe et al., 2012; Salazar et al., 2012).

However, to study the relation between large-scale network dynamics and behavior multi-site implants are required that permit simultaneous recordings from extended sets of distributed brain

areas. Such recordings can be carried out using electrocorticographic (ECoG) arrays which have, beyond their clinical application, gained in importance in the study of functional network connectivity in recent years (Crone et al., 2006; Bosman et al., 2012; Keller et al., 2014; Fukushima et al., 2015; Lewis et al., 2015).

Here, we have employed an ECoG approach to study large-scale functional connectivity, as reflected in phase coupling of neural oscillations, underlying spatial multisensory processing. Studies on the relation between phase coupling and multisensory interaction are rare in humans (Keil et al., 2014; Giordano et al., 2017). In animal studies, the potential role of functional connectivity involved in multisensory interactions has so far been investigated only by multielectrode recordings from the same cortical areas (Lakatos et al., 2007; Kayser et al., 2008) or by simultaneous recordings from at most two different regions (Ghazanfar et al., 2008). We have now investigated dynamics during multisensory processing in a large-scale cortical network involving visual, auditory, somatosensory and parietal areas using 64-channel ECoG recordings in behaving ferrets.

Ferrets were trained in a 2-alternative-forced-choice paradigm to detect brief auditory and visual stimuli presented either left or right from the midline. We hypothesized that fluctuations in coupling, indicative of dynamic variations in the network state, should be predictive of the animals' performance. Separate analysis of power for hit and miss trials revealed significant differences around stimulus and response onset but not for the baseline period before stimulus onset. In contrast, phase coupling already differed between hits and misses at the baseline, suggesting that fluctuations in network state are an important factor that determines task performance. Analysis of the topography of connectivity differences between hits and misses suggested specific patterns. In particular, higher phase coupling of visual and auditory regions with parietal cortex was predictive of task performance. Furthermore, we observed that long-range coupling became more predominant during the task period compared to the pre-stimulus baseline. Our results suggest that fluctuations in the networks state, particular with respect to long-range connectivity, are critical for task performance during multisensory processing.

Results

To investigate neural responses and task-related fluctuations of functional connectivity, we recorded local field potentials (LFPs) via 64-channel ECoG arrays chronically implanted in four female ferrets performing an audio-visual detection task (Hollensteiner et al., 2015). Initially, the animals were handled and accustomed to the experimental setup. Subsequently, they were trained in the detection task (Fig. 1) to determine unimodal and bimodal psychophysical thresholds, which were quantified by logistic fits to the response statistics (Fig. 2A). The ECoG was implanted after successful training and LFP recordings during execution of the acquired behaviors were carried out.

Behavioral data

The task involved four different types of trials. Stimulus presentation could be unimodal visual (V), unimodal auditory (A) or a spatiotemporally congruent bimodal audio-visual stimulus combination. The bimodal combination either consisted of an auditory stimulus of variable amplitude accompanied by a visual stimulus of constant contrast (Av) or, conversely, a visual stimulus of varying contrast accompanied by an auditory stimulus of constant amplitude (Va). The intensity value of the constant stimulus from the respective second modality was set at a level of 75% detection accuracy as determined during unimodal stimulation. Figure 2 shows an example for the psychometric functions fitted to the behavioral data for the four conditions. For further analysis, data were taken only from trials with stimulus intensities at threshold to allow comparisons across conditions and animals (Fig. 2A,B).

To investigate reaction time (RT) difference between unimodal and bimodal trial types, a paired sample *t*-test between was run between Av and A, as well as between Va and V trials, respectively. Responses to bimodal stimulation were, on average, faster than those to unimodal stimulation ($p<0.05$). To evaluate whether this effect was driven by the audio or the visual condition, we computed a repeated one-way analysis of variance (rm-ANOVA), with sensory modality as a main factor. This revealed a main effect of condition ($F(3,12) = 5.3$, $p<0.05$), but post hoc *t*-tests (Bonferroni corrected) only revealed significant differences between the A trials and all other conditions. The population averages of RTs for Av, Va and V were not significantly different (Fig.

2B). Nevertheless, the population RT mean of V (0.21 sec) was slightly higher compared to Va (0.19 sec) and Av (0.19 sec). The significant difference between the RTs in the A and the Av condition suggest that there was a multisensory interaction effect leading to improved performance for the bimodal stimulation. However, our data do not suggest a substantial improvement of visual detection by a concurrent auditory stimulus.

A major aim of our analysis of the electrophysiological data was to test the relation of power and functional connectivity to task performance. To this end, we contrasted hit and miss trials. In the hit trial group, we included all trials with stimulus intensities around 75 % threshold and stimulation contralateral to the implanted ECoG (265±14 hit trials per animal, mean±SEM). To match the number of hit trials we used all miss trials (236±45 miss trials per animal) throughout all sessions (15±2 sessions per animal). Miss trials were defined as trials with sensory stimulation but without behavioral response, i.e., the ferret maintained the centered head position throughout the response window. The number of false responses, i.e., orientation of the ferret to the side contralateral to the sensory stimulation, were too few and highly variable across animals (104±58 false responses per animal). Therefore, these trials were not included in analysis of the electrophysiological data.

LFP power reflects stimulus processing and response preparation

We hypothesized that spectral characteristics of LFPs immediately before task execution might predict the animal's performance. To assess how LFP spectral characteristics evolve during hit, miss and bi- and unimodal stimulation, we computed the power across in analysis time windows aligned to trial-, stimulus- and response-onset for each animal individually (Fig. 3). Results of all animals were pooled after correction for different trial numbers. Power differences between hit and miss trials were analysed in the theta (4-8 Hz), alpha (8-16 Hz), beta (18-24 Hz), gamma (30-80 Hz) and high-gamma (80-160 Hz) frequency band across the analysis time windows (Tab. 1). In addition, one-way ANOVAs were calculated on power values within each frequency band with condition as the main factor to examine differences related to stimulus type (Suppl. Fig. 1; Suppl. Tab. 1).

Figure 3 shows the grand average spectra and time-frequency representation of power changes during each analysis time window (baseline, stimulus and response onset) for hit and miss trials.

During the baseline only the high-gamma frequency-band (80-160 Hz) showed differences with higher power for miss trials ($p<0.05$; FDR corrected). Comparison of the average spectra in the stimulus onset analysis window showed significant reductions for hit and miss trials in the gamma frequency-range (30-160 Hz) compared to baseline (Fig. 3C, Tab. 1). However, hit trials showed significantly higher power compared to miss trials after stimulus onset in both gamma ($p<0.001$) and high-gamma ($p<0.001$) frequency bands (Fig. 3B). Around response onset, hit trials consistently showed significantly higher power compared to miss trials in the theta- ($p<0.01$), alpha- ($p<0.01$), gamma- ($p<0.001$) and high-gamma band ($p<0.001$). Statistical comparison across analysis time windows within hit- and miss-trials revealed significant de- and increase in the gamma frequency range compared to baseline and stimulus onset, respectively (Tab. 1; all *p*-values, within and across windows of interest, FDR corrected).

Supplementary Figure 2 shows the topographies of the respective spectral differences between hit and miss trials. In the baseline window, power topographies showed high spatial uniformity across all frequency bands. Around stimulus onset, notable differences occurred mainly in the beta band where, in hit trials, higher beta power occurred in parietal areas. Interestingly, highest regional differences occurred in the response window. Occipital regions exhibited higher power across all frequency bands during response onset in miss trials compared to hit trials. In contrast, auditory and parietal areas showed increased power in lower frequency bands (theta and alpha) for hit trials. An increase of gamma band power occurred in the response window for hit trials in regions around the lateral sulcus (Suppl. Fig. 2).

To investigate stimulus-type dependent effects within hit-trials a one-way ANOVA between the four conditions (Av, Va, A and V; Suppl. Fig. 1; Suppl. Tab. 1) was calculated. It showed no main effect in the factor condition across frequency bands during baseline, stimulus or response onset. This suggests that power changes related to stimulus processing and response preparation did not depend on the modality of the presented stimulus or on crossmodal interactions.

Functional connectivity predicts performance

To determine whether functional connectivity predicts the animals' performance we computed the PLV between all pairs of ECoG channels for the different frequency bands. PLV analysis was performed for the same time windows, aligned to baseline, stimulus and response onset, respectively, as the power analysis reported above. Figure 4 displays the population average PLV spectra for all hit and miss trials as well as the difference between hits and misses and the relative spectral changes in the stimulus and response onset window relative to baseline. Paired *t*-tests were applied between hit and miss trials within and across all time windows for each frequency band. Within each analysis window, significantly higher PLV was observed for hits compared to miss trials in all frequency bands, with exception of the theta band during response onset ($p<0.05$, FDR corrected) (Fig. 4A).

When compared to the baseline time window, PLV was significanctly reduced in the stimulus and response onset windows in nearly all frequency bands. Exceptions were in the theta frequency band for miss trials around stimulus as well as response onset. From stimulus to response onset, there was an increase in alpha PLV and a decrease of gamma PLV for hit trials, as well as a significant decrease in high-gamma PLV for both trial groups (Fig. 4A and Tab. 2).

A one-way ANOVA within analysis time windows and frequency bands with Condition as the main factor revealed differences in PLV between stimulation conditions (Av, Va, A and V; Suppl. Fig. 3). During the baseline period there was no significant effects in the main factor condition in the theta frequency band ($F(3, 44) = 2.46$, $p>0.05$). However, starting with the alpha ($F(3, 76) = 4.98$, $p=0.003$), beta ($F(3, 60) = 3.71$, $p=0.016$), gamma ($F(3, 412) = 31.89$, $p<0.001$) and high-gamma ($F(3, 652) = 56.99$, $p<0.001$) frequency bands, there was a main effect in Conditions. This effect persisted also for the windows around stimulus onset (theta: $F(3, 44) = 1.23$, $p>0.05$; alpha: $F(3, 76) = 3.74$, $p=0.015$; beta: $F(3, 60) = 3.5$, $p=0.021$; gamma: $F(3, 412) = 26.12$, $p<0.001$; high-gamma: $F(3, 652) = 55.67$, $p<0.001$) and response onset (theta: $F(3, 44) = 2.31$, $p>0.05$; alpha: $F(3, 76) = 3.63$, $p=0.017$; beta: $F(3, 60) = 3.67$, $p=0.017$; gamma: $F(3, 412) = 25.12$, $p<0.001$; high-gamma: $F(3, 652) = 51.24$, $p<0.001$). Furthermore, post hoc *t*-test confirmed a constant pattern of significant differences between conditions (Suppl. Tab. 2-4). Interestingly, for hit trials connectivity was higher in the A and Av

conditions than in the V condition, and there was a trend for connectivity in bimodal Va trials to be higher than in unimodal V trials (Suppl. Fig. 3).

In summary, our analysis of functional connectivity revealed significant differences between hits and misses already in the baseline period. The differences between hit and miss trials in PLV occurred over a broad range of frequencies across all analysis time windows. Importantly, this is in contrast to the power differences between hits and misses, which were not observed before stimulus onset and spectrally more confined. This suggests that the observed power changes predominantly reflect differences in local computations within sensory systems, whereas the changes observed in PLV indicate fluctuations in network state involving multiple frequency bands that relate to the animals' performance.

Large-scale coupling shows specific changes during the task

To examine functional connectivity in relation to the topography of cortical areas, we assigned the data of each ECoG contact to a distinct region based on the functional map of cortical areas from Bizley et al. (2007) (see Methods) and constructed functional connectivity matrices accordingly (Fig. 5). Cortical areas were grouped in three functional systems, comprising visual (areas 17, 18, 19, 20, 21), auditory (areas A1, AAF, ADF, PPF and PSF), and parietal areas (SSY, PPc, PPr, S2). Differences between hit and miss trials were expressed using the sensitivity index (d').

In line with the grand average PLV results, the connectivity matrices generally display positive d' values and, thus, higher functional connectivity for hit compare to miss trials. (Fig. 5). This effect was most prominent during the baseline window and decreased during the stimulus window. For the alpha, gamma and high-gamma band, the PLV difference between hit and miss trials increased again in the response window. Generally, connections between early sensory cortices and parietal cortex displayed the highest differences between hit and miss trials, in particular during the baseline window (Fig. 5; Suppl. Fig. 4).

The topography of functional connectivity changes was further analyzed by contrasting between-system and within-system interactions (Fig. 6; Suppl. Fig. 4). For hit trials, interactions between the three functional systems were stronger than functional connections within the respective

system. Regarding the within-system connectivity, the auditory system showed the lowest d'. In the period from baseline to stimulus-onset, the strength of d' decreased across all frequency bands. With response onset the spectral profile of d' became more heterogeneous. In the theta-band d' decreased further, whereas it remained unaltered in the beta-band, and increased in the alpha-, gamma- and high-gamma band.

For statistical analysis, we averaged PLV d' values and derived the difference of d' values between long-range (between-system) and short-range (within-system) connectivity and calculated statistics across analysis time windows for each frequency band (Fig. 6; for statistics across systems and within analysis time windows and frequency see Suppl. Fig. 4 and Suppl. Tab. 5; for modality specific statistics see Suppl. Fig. 5). To reveal dynamic effects within frequency bands of interest a one-way ANOVA with time window as the main factor was computed. There was no main effect in the theta band ($F(2, 6) = 4.39$, $p>0.05$). The ANOVA exposed significant effects for the main factor time window (alpha ($F(2, 12) = 17.17$, $p<0.001$; beta ($F(2, 9) = 14.43$, $p=0.002$; gamma ($F(2, 75) = 3.71$, $p<0.001$; high-gamma ($F(2, 120) = 17.94$, $p<0.001$). Post hoc t-tests revealed significant differences between baseline and stimulus-onset for all frequency bands with the main effect (alpha: $p=0.011$; beta: $p=0.002$; gamma: $p<0.001$; high-gamma: $p<0.001$), between stimulus and response onset for the gamma frequency range (gamma: $p=0.009$; high-gamma: $p<0.001$) and between baseline and response-onset in the alpha- ($p<0.001$) and beta- ($p=0.006$) frequency bands (Bonferroni corrected).

Taken together, comparison of functional connectivity between and within cortical systems across the different analysis time windows revealed that between- compared to within-system connectivity was stronger during the task period compared to the pre-stimulus baseline. In hit trials, phase coupling was higher between systems in the gamma frequency range during stimulus onset compare to baseline and response onset. Furthermore, low frequency (alpha and beta) coupling between systems increased around response onset in hit trials compared to miss trials. These results suggest that fluctuations in the networks state, particular with respect to long-range connectivity, are related to task performance.

Discussion

This study has aimed at investigating the cortical network dynamics underlying performance in a multisensory detection task. The main focus of our analysis was on the relation between functional connectivity and task performance. We have used an ECoG approach to record a large-scale network comprising visual, auditory, somatosensory and parietal areas in behaving animals over extended time periods. We hypothesized that fluctuations in power and coupling, indicative of dynamic variations in the network state, should be predictive of the animals' performance. In line with this hypothesis, our data show that pre-trial baseline connectivity predicts the animals' performance, suggesting that fluctuations in coupling across the network lead to variability in behavior. In contrast, local signal power in the pre-trial baseline does not predict hits and misses. Analysis of the topography of connectivity differences between hits and misses suggested specific patterns. In particular, higher phase coupling of visual and auditory regions to parietal cortex was predictive of task performance. Furthermore, we analyzed the ratio between long- and short-range functional connectivity across the different task phases. We observed that long-range coupling became more predominant during the task period compared to the pre-stimulus baseline and changed its spectral profile over the course of the trials.

Investigating large-scale network dynamics

A large number of studies have shown that large-scale functional connectivity is highly relevant for cognition and behavior (Engel et al., 2001; Varela et al., 2001; Fries, 2005; Engel and Fries, 2010; Siegel et al., 2012). In particular, phase coupling has been suggested to serve the routing of information through cortical networks and to promote selective communication between distant brain areas (Engel et al., 2001; Fries, 2005; Womelsdorf et al., 2007). In the human brain, studies of large-scale network dynamics have remained challenging, although substantial advances have been made with non-invasive methods such as EEG or MEG (Brookes et al., 2011a; Siegel et al., 2012; Engel et al., 2013; O'Neill et al., 2017). In animal studies, a substantial number of investigations have addressed functional connectivity between distant populations, but these have typically been restricted to recordings from a relatively small number of sites (Buschman and Miller, 2007; Gregoriou et al.,

2009; Salazar et al., 2012). However, in order to capture large-scale network dynamics and fluctuations of functional connectivity across multiple regions, implants are required that permit simultaneous recordings from extended sets of brain areas.

To this end, ECoG arrays have gained importance in recent years (Crone et al., 2006; Keller et al., 2014; Fukushima et al., 2015; Lewis et al., 2015). Beyond their clinical application, ECoG arrays are ideally suited for the study of functional connectivity in networks underlying cognitive and sensorimotor functions. In patients, phase coupling across brain areas has been investigated using ECoGs in a variety of perceptual and cognitive tasks, providing supportive evidence for the notion that long-range synchronization of oscillatory signals has a functional role (Canolty and Knight, 2010; Fox et al., 2018). In monkeys, ECoG recordings have been applied to study phase coupling between early and higher-order visual areas serving attentional selection (Bosman et al., 2012; Bastos et al., 2015). In rodents, ECoG approaches have been employed to investigate patterns of synchrony in visual cortex (Toda et al., 2018). We have recently used ECoG implants to investigate phase coupling during spontaneously occurring state changes in the ferret (Stitt et al., 2017).

For studies chronically implanted animals, ECoG arrays are advantageous because of the long-term stability of the implant and the recorded signals (Rubehn et al., 2009; Bosman et al., 2012; Bastos et al., 2015; Stitt et al., 2017). Thus, they permit repetitive and long-term tracking of brain activity and the investigation of spatiotemporal neural patterns under a broad variety of experimental conditions. Another advantage is the higher signal-to-noise ratio of the recorded local field potential signals. Furthermore, it has been shown that high-resolution ECoG arrays with sufficiently small contacts also permit the recording of spikes from the cortical surface (Khodagholy et al., 2016; Bockhorst et al., 2018).

Despite the fact that the ECoG array in this study covered only the posterior half of the cortical hemisphere, it enabled us to record from an extended network of cortical areas involving visual, auditory, somatosensory and parietal areas, allowing to investigate large-scale network dynamics during trained behavior over a large number of recording sessions. In addition to the advantages mentioned above, a key feature in the present study was the possibility to simultaneously monitor several different functional systems. Since our micro-ECoG array also allowed recordings

from multiple areas within the same cortical system, this approach enabled a systematic comparison of within-system and between-system functional connectivity as a function of the animals' behavior.

Relation of large-scale connectivity to task performance

A key goal of this study was to investigate the relation between phase coupling and performance of the animal in the detection task, with the aim to provide further evidence for the functional relevance of synchrony across cortical populations. A number of different approaches have been used to capture the relation between large-scale connectivity and task performance. In humans, phase coupling has been increasingly studied using EEG or MEG in recent years (Fell and Axmacher, 2011; Siegel et al., 2012; O'Neill et al., 2017), enabled by progress in source localization techniques and in connectivity methods that allow to remove spurious coupling resulting from volume conduction (Nolte et al., 2004; Gross et al., 2001; Brookes et al., 2011a; Hipp et al., 2012). Using these approaches, coherence of different brain areas has been observed during cognitive tasks involving perceptual selection (Hipp et al 2011), attentional selection (Siegel et al., 2008; Michalareas et al., 2016), working memory (Brookes et al., 2011b) or speech processing (Giraud and Poeppel, 2012; Giordano et al., 2017).

Animal investigations have elucidated the relation between large-scale connectivity and task performance on different spatial and temporal scales. Early studies performig multi-site recordings in chronically implanted animals demonstrated a relation of neural synchrony to sensorimotor processing (Bernasconi et al., 2000; Roelfsema et al., 1997). Long-range phase coupling in various frequency ranges has been shown to be related to attentional selection and working memory processes in the monkey (Gregoriou et al., 2009; Salazar et al., 2012; Liebe et al., 2012; Bosman et al., 2012; Saalmann et al., 2012; Bastos et al., 2015). Importantly, recordings in monkeys suggest that feedforward and feedback signaling between cortical areas are mediated by distinct frequency channels, i.e., gamma coupling is likely to subserve feedforward whereas lower-frequency coupling seems to be involved in feedback signaling (Buschman and Miller, 2007; Bastos et al., 2015).

Our ECoG approach enabled us to investigate dynamic large-scale connectivity between functional cortical systems during a spatial detection task. Our data show that phase coupling, in contrast to local power, is already different between hit and miss trials in the pre-trial baseline,

suggesting that fluctuations in network state may be an imported factor that determines task performance. The data indicate that stronger phase coupling in the network may lead to higher efficiency of stimulus processing and response preparation. This is in line with earlier studies that have demonstrated that increased synchrony enhances communication across brain areas, e.g., in the context of attention (Fries, 2005; Bosman et al., 2012). Enhanced functional connectivity seems important to link task-relevant modalities to areas involved in selection of responses (Siegel et al., 2012; Miller and Buschman, 2013). Indeed, we find that stronger phase coupling of early sensory to parietal areas was predictive of task performance (Suppl. Fig. 4).

Interestingly, no clear frequency specificity was apparent in performance-predictive phase coupling as observed in previous studies. We did not observe the typical signatures of vigilance- or attention-related fluctuations characterized by an increase in higher frequency components and a decrease in low frequenciy bands (Hanslmayr et al., 2007; Siegel et al., 2008; Bosman et al., 2012). Importantly, we also did not observe classical signatures of arousal changes in local signal power, since we did not see spectral differences between hit and miss trials in the pre-stimulus baseline in the recorded cortical areas.

Although the average connectivity differences between hits and misses had a rather broad spectral profile, a closer analysis of the contrast between long-range and local connections revealed an interesting pattern (Fig. 6). The comparison of functional connectivity between and within cortical systems across the different analysis time windows revealed that long-range compared to short-range connectivity was stronger during the task period compared to the pre-stimulus baseline. In hit trials, between-system phase coupling in the gamma frequency range was higher during stimulus onset compared to baseline and response onset. In contrast, in low frequency (alpha and beta) ranges between-system coupling increased around response onset in hit trials compared to miss trials.

Although we did not employ directed connectivity measures such as Granger causality to distinguish between bottom-up and top-down information flows (Bastos et al., 2015), these data suggest the possibility that, during stimulus processing, higher frequency interactions predominate in successful trials, which might reflect stronger bottom-up signaling. This could relate to attentional gating, allowing information to pass through the network to higher areas. In contrast, the

predominance of low-frequency interactions in the epoch around reponse onset might indicate stronger top-down information flow (Bastos et al., 2015). Alternatively, in that phase of the trial, parts of the network could already return to a default state dominated by low frequency oscillations. Analysis of directed connectivity would be required to further test these hypotheses. Averaged across areas, spectral differences between connections with dominant bottom-up and top-down information flows might average out and, thus, yield the broad spectral profile of connectivity changes observed in the present analysis.

Functional connectivity and multisensory processing

As discussed above, dynamic functional coupling likely constitutes a mechanism for integration of distributed neural signals. This holds, in particular, for perceptual integration within individual sensory modalities (Singer and Gray, 1995; Singer, 1999; Engel et al., 2001; Fries, 2005; Arnal et al., 2015; Ploner et al., 2017). It has been suggested that similar mechanisms might operate for the integration of information across different sensory systems. Thus, multisensory interactions might involve dynamic coupling of oscillatory signals arising in different cortical systems (Senkowski et al., 2008; Talsma et al., 2010). In the human brain, the vast majority of studies on neural oscillations and crossmodal processing have focused on local power changes, and only few investigations have addressed the relation between multisensory processing and functional coupling (Keil et al., 2014; Giordano et al., 2017). Using a data-driven approach for analysis of functional coupling in the human EEG, we could recently demonstrate that coherence in networks involving parietal and sensorimotor areas predicts performance in a visuotactile matching task (Wang et al., 2018).

A number of studies in monkeys have investigated functional connectivity during multisensory tasks. Thus, simultaneous recordings from auditory cortex and superior temporal sulcus revealed increased coherence during congruent auditory and visual stimulation (Maier et al., 2008). Another study showed that interactions mediated by coherent gamma band oscillations between these areas are involved in crossmodal integration of information related to faces and voices (Ghazanfar et al., 2008). An interesting mechanism that might also contribute to multisensory integration has been suggested by studies demonstrating that phase-resetting of oscillatory activity in sensory areas can

occur under the influence of stimuli from a different sensory modality (Lakatos et al., 2007; Kayser et al., 2008; Schroeder and Lakatos, 2009).

While these in-vivo studies investigated multisensory interactions only by recordings from the same cortical areas or by simultaneous recordings from at most two different regions, our study has addressed multisensory networks at a larger scale involving visual, auditory and parietal cortical regions. While our data clearly demonstrate a relation of functional connectivity to task performance, we did not obtain evidence for stimulus-specific changes of coupling between visual and auditory areas. Behaviorally, we observed audiovisual interaction effects reflected in a shortening of reaction times for bimodal compared to unimodal stimulus detection. However, there were no strong connectivity difference related to these multisensory interaction effects. Rather, our findings show broadband coupling between visual, auditory and parietal areas, which gets stronger before hits compared to instances where the animal fails to detect the stimulus. Interestingly, connectivity in auditory hit trials was higher than in visual hit trials and, in the visual conditions, there was a trend for higher connectivity in bimodal compared to unimodal trials (Suppl. Fig. 3).

The absence of profound connectivity effects related to multisensory interaction may relate to the nature of the task used in our study, which did not require integration of features across modalities, but only the rapid detection of highly transient stimuli. Nonetheless, our connectivity data support the notion that significant functional coupling can occur already between early sensory areas, suggesting that multisensory integration can already occur at early processing stages and does not solely rely on binding of information at higher processing levels (Bizley et al., 2007; Lakatos et al., 2007; Senkowski et al., 2008). This is in line with anatomical data suggesting that direct projections from primary auditory to visual cortices can enable functional coupling supporting early multisensory interactions (Bizley et al., 2015).

Network state and behavioral variability

A key result of our study is that phase coupling differed between hit and miss trials already in ongoing activity before stimulus onset. Interestingly, local power in the pre-trial baseline did not differ between hits and misses. Our data suggest that fluctuations in the network state occur which lead to variability

in the animals' behavior, and that these state changes are primarily reflected in shifts of long-range connectivity, rather than changes in the dynamics of local populations.

Variability in ongoing activity has been addressed in numerous studies which showed that pre-stimulus activity can influence sensory processing and behavior. Early studies assumed that ongoing neural activity corresponds to noise resulting from random signal fluctuations without any functional relevance (Zohary et al., 1994; Shadlen et al., 1996). However, this view is defeated by evidence showing that ongoing activity carries information and can shape the processing of stimuli (Arieli et al., 1996; Galindo-Leon et al., 2019). Abundant evidence is available that oscillatory temporal patterning of ongoing activity is important for sensory and cognitive processes (Busch et al., 2009; Keil et al., 2014). One relevant mechanism is that the ongoing neuronal oscillations can amplify or diminish local responses depending on whether inputs arrive during phases of high or low excitability (Fries et al., 2001; Engel et al., 2001; Lakatos et al., 2007). Such fluctuations of ongoing activity do not occur only locally, but are strongly synchronized across spatially distributed neuronal populations (Steriade et al., 1996; Stitt et al., 2017; Fischer et al., 2018).

Phase coupling of oscillations in pre-stimulus epochs has been shown both in animal and human studies to predict perception and performance in cognitive tasks. For instance, studies in monkey visual cortex indicate that fluctuations in gamma-band phase coupling modulates the speed at which animals can detect a behaviourally relevant stimulus change (Womelsdorf et al., 2006). EEG studies in humans provide convergent evidence that pre-stimulus fluctuations in phase coupling can modulate target detection (Hanslmayr et al., 2007). Furthermore, intrinsic fluctuations of phase coupling is associated with fluctuations in perceptual states in ambiguous stimulus settings. Fluctuations in beta-band or gamma-band phase coupling have been shown to predict the perceptual state in ambiguous sensory paradigms (Rose and Büchel, 2005; Hipp et al., 2011) and decision making in near-threshold stimulation regimes (Donner et al., 2009). Our current results corroborate and extend this evidence by showing that, at perceptual threshold, detection of the lateralized stimuli by the animals is biased by phase coupling in the pre-stimulus interval. A novel element in our approach is the ability to simultaneously monitor numerous cortical areas, enabling us to quantify within-system and between-system interactions and to characterize these in a spectrally resolved manner. Our

analysis showed that, in particular, long-range connectivity between different functional systems was related to successful stimulus detection. This is in line with the hypothesis that long-range phase coupling may serve efficient transmission of task-relevant information in sensorimotor networks (Engel et al., 2001; Fries, 2005; Womelsdorf et al., 2007).

Our results also support the view that characterization of brain state changes strongly benefits from inclusion of connectivity analyses. The observation that changes in network state are reflected, in particular, in fluctuations of large-scale connectivity is in line with results of other recent studies. Supportive evidence has been obtained in studies on the human brain (He et al., 2008; Supp et al., 2011). Using the same ECoG recording approach for the study of ongoing activity, we have observed that functional connectivity shows state-dependent reconfiguration which can also involve shifts in the ratio between short- and long-range interactions (Stitt et al., 2017; Fischer et al., 2018). These findings raise the question of possible mechanisms that might modulate large-scale functional connectivity in a state- and task-dependent manner. Possible candidates are changes in the output of ascending neuromodulatory systems (Harris and Thiele, 2011). Phase coupling has long been known to be influenced by neuromodulators (Steriade et al., 1993). For instance, activation of cholinergic brain stem nuclei has been shown to enhance gamma-band phase coupling in cortical networks (Munk et al., 1996). Neuropharmacological evidence suggests, furthermore, that noradrenergic brain stem inputs can modulate large-scale functional connectivity in cortex (van den Brink et al., 2018).

Conclusion

Our study has demonstrated functional coupling across visual, auditory and parietal areas during a lateralized detection task in the ferret. Analysis of power for hit and miss trials revealed significant differences around stimulus and response onset. In contrast, phase coupling already differed between hits and misses at baseline, suggesting fluctuations in large-scale network connectivity. In particular, higher phase coupling of visual and auditory regions to parietal cortex was predictive of task performance. We observed that long-range coupling became more predominant during the task period compared to the pre-stimulus baseline. Taken together, these results suggest that fluctuations in the network state, particular with respect to long-range connectivity, are critical determinants of the

476 animals' behavior. Future studies might address the relation to the underlying structural connectivity
477 and the mechanisms that give rise to the observed variability of phase coupling. Furthermore, analyses
478 of directed coupling might elucidate the interplay of bottom-up and top-down interactions during
479 network states predictive of task performance.

Materials and Methods

Animals

Data were recorded in four adult female ferrets (*Mustela putorius furo*) trained on a two-alternative forced-choice task involving lateralized detection of visual and auditory stimuli that we have established previously (Hollensteiner et al., 2015). All experiments were approved by the independent Hamburg state authority for animal welfare (BUG-Hamburg) and were performed in accordance with the guidelines of the German Animal Protection Law.

Sensory stimulation

All experiments were carried in a dark sound-attenuated chamber (Acoustair, Moerkapelle, Netherlands). Visual and auditory stimuli were generated with the Psychophysics Toolbox (Brainard, 1997). Visual stimuli were presented on an LCD monitor (Samsung SyncMaster 2233, frame rate 100 Hz) placed 20cm in front of the animal. Auditory stimuli were generated digitally with a sample rate of 96 kHz and delivered through two Beyerdynamic T1 speakers. Auditory stimuli consisted of white noise bursts of 100 ms duration and were presented with intensities between 2 to 62 dB SPL. Visual stimuli consisted of circular gratings (22.5 °, 0.2 cycles / °, 5 Hz) with Michelson contrast (Cm) between 0 and 0.38. A static random noise pattern located in the center of the screen was presented to indicate trial onset by a decrease in contrast. Multisensory stimuli consisted of both stimulation types presented simultaneously.

Training

Initially, ferrets were handled and accustomed to the experimental setup (Fig. 1A). Subsequently, they were trained in the spatial detection task, and unimodal as well as crossmodal psychophysical thresholds were estimated. In the task, we used a crossmodal approach that bears on established unimodal training paradigms (e.g. Nodal et al., 2008). Animals were restricted from access to water for a period of 8 hours before the measurements, and conditioned by using water rewards during the task. In the first phase of the study, the animals were trained to detect unimodal auditory and visual stimuli presented in a randomized fashion. Auditory and visual unimodal detection thresholds were

508 determined using 20 different stimulus amplitudes (auditory: 2-62 dB SPL; visual: 0-0.38 Cm) in a 1
509 down / 3 up staircase procedure (Kaernbach, 1991). Next, unimodal and bimodal thresholds were
510 assessed in a combined approach, using the previously determined unimodal thresholds to adjust the
511 test parameters (for details of the procedure see Hollensteiner et al., 2015). Subsequently, the ferrets
512 were accustomed to electrophysiological recordings during the detection task with a reduced set of
513 stimulus amplitudes (eight per modality), adjusted to the individual psychometric functions to acquire
514 a higher number of trials in the performance range of interest around 75% accuracy.
515

516 **Detection task**

517 The trial schedule of the detection task is shown in Figure 1B and 3A. To initialize a trial, the ferret
518 had to maintain a central head position to break the central light-barrier for 500 ms. This caused the
519 static random noise pattern in the center of the screen to decrease in contrast informing the animal that
520 the window for stimulus presentation (from 0 to 1000 ms after trial onset) had started. During this
521 interval, the animal had to further maintain its central head position. A stimulus was presented for 100
522 ms on either the left or the right side. Stimulus presentation could be unimodal visual ('V'), unimodal
523 auditory ('A') or a temporally congruent bimodal audio-visual stimulus combination. This
524 combination either consisted of a variable auditory stimulus accompanied by a visual stimulus of
525 constant contrast ('Av') or, conversely, a visual stimulus of varying contrast supported by an auditory
526 stimulus of constant amplitude ('Va'). The intensity value of the accompanying second stimulus with
527 constant amplitude was set at a level of 75% accuracy. After stimulus offset, the animal had to respond
528 within 700 ms by moving its head to the stimulated side; otherwise, the trial was considered as a miss
529 (no response). If the response was correct the animal received a water reward (~80 µl) from a spout at
530 the stimulus position and could immediately start the next trial. If the response occurred prematurely
531 (before stimulus onset or within 100 ms after stimulus onset), was incorrect (wrong side) or omitted
532 (no response), the trial was immediately terminated, followed by a 2000 ms interval during which no
533 new trial start could be initialized.

Implantation and alignment of ECoG array

Micromachining technology (Rubehn et al., 2009) was used to design and implement an ECoG array that matched the anatomy of the ferret brain (Fig. 7). Each thin-film (10µm) polymide-foil ECoG contained 64 platinum electrodes with a diameter of 250 µm, each, arranged in a hexagonal formation at an inter-electrode distance of 1.5 mm.

The surgical procedure for the implantation of the ECoG array started with an initial injection of anesthesia (ketamine 15 mg/kg and medetomidine 0.08 mg/kg) and additional ketamine (20 mg/kg) was supplied during surgery. The animal was freely breathing throughout the implantation. Physiological parameters such as the electrocardiogram (ECG) and rectal temperature were monitored throughout the surgery. All surgical procedures were performed under sterile conditions. After the operating field was prepared, a craniotomy was performed using a saline-cooled ultrasonic microsaw (Mectron) in order to expose the posterior half of the left cerebral hemisphere. The dura was carefully removed and the ECoG array was gently placed on the surface of the cortex such that it covered occipital, temporal and parietal areas (Fig. 7D). The dura was then folded back over the ECoG array and an absorbable artificial dura was placed above the ECoG, covering the trepanation to full extent. The excised piece of bone was fixed back in place with titanium plates and screws and subsequently the gaps were filled with fast set absorbable bone putty. Finally, the ECoG's connector was placed on top of the skull and fixed in place with titanium screws and dental acrylic. After the surgery, the animals received analgesics (carprofen, 4mg/kg) and antibiotics (enrofloxacin, 5 mg/kg) for at least 7 days. To align electrode positions across animals, the ECoG array placement and the cortical parcellation introduced by Bizley et al. (2007) was utilized (Fig. 7B). For each animal, the exact ECoG array position over the posterior cortex was photographically documented during surgery. The locations of all 64 ECoG electrodes were then projected onto a scaled illustration of a ferret model brain. Each electrode was then mapped to the underlying cortical area.

Electrophysiological recordings

Local field potentials (LFPs) were digitized at 1.4 kHz and sampled simultaneously with a 64-channel AlphaLab SnR recording system (Alpha Omega Engineering, Israel). The high pass filter was set at 0.1 Hz and the low pass filter at 357 Hz.

Data analysis and preprocessing

To reveal dynamic neurophysiological processes along the trial time line, we analyzed spectral power and functional connectivity in the LFPs recorded during the task. To ensure comparability across animals and modalities, only trials with an accuracy of 75±10 % were considered in all electrophysiological analyses. Furthermore, this selection of trials ensured better comparability between all four modalities because the value that was fixed during the bimodal stimulation was set at a level of 75 % accuracy for all stimulation amplitudes. To assess a sufficient amount of right side trials (i.e., trials with stimulus presentation contralateral to the implanted hemisphere) per modality in the 75 % accuracy range, trials collected on different days were pooled; see Hollensteiner et al. (2015) for non-stationarity effects across sessions.

All offline data analysis was performed using custom scripts in Matlab (The Mathworks Inc, MA). The hardware-filtered LFP signals were band-pass filtered with a phase-preserving fourth-order Butterworth filter between 2 and 200 Hz. Next, band-stop Butterworth filters at 49-51, 99-101 and 149-151 Hz were applied to notch the line noise. Following, the continuous LFP signals were cut into epochs aligned to trial, stimulus and response onset. In each of these analysis time windows data was cut from 500 ms pre- to 500 ms post-onset, with 500 ms real data padding on each side to prevent edge artifacts in frequency space. Afterwards, we applied independent component analysis (Hyvärinen and Oja, 2000) to the concatenated analysis window data in order to detect ECG, muscle and eye blink artifacts. Subsequently, we re-referenced the LFP time series of each ECoG contact with the LFP time series of its right neighbor. This processing step created 55 virtual electrodes from the 64 recorded contacts. The virtual electrode position was derived from the difference of both real electrode positions. Subsequently, the oscillatory signal components of unimodal and bimodal trials where analyzed using spectral decomposition.

Spectral power analysis

Channel-wise spectral power was computed by taking the square of the absolute value of time frequency estimates. Spectra were computed for all three analysis time windows using a Hanning window approach (2-200 Hz, 2 Hz steps, 500 ms window; for the LFP spectrogram the window was shifted from –500 ms to 500 ms around the window of interest) in 1 ms steps.

Functional connectivity

To estimate phase synchronization between ECoG signals, we calculated the PLV (Lachaux et al., 1999) across all frequencies (2-200 Hz). In general, the instantaneous phase θ was extracted from the analytic signals that were produced by the Fourier transform of the convolution of the ECoG time series with the Hanning window. The PLV between channels A and B at carrier frequency f is defined as follows:

$$PLV_{AB}(f) = \frac{1}{N}\left|\sum_{n=1}^{N} e^{i(\theta_n^A(f)-\theta_n^B(f))}\right|$$

At first, PLV was computed between all pairs of ECoG electrodes. To contrast PLV between modalities, we first computed the global mean PLV for the same time windows selected in the spectral power analysis. Subsequently, the PLV between anatomical regions, as defined in Figure 7B, was calculated by averaging across all virtual electrodes overlaying the same area. To normalize and compare PLV values from hit and miss trials we computed the sensitivity index (d'), which is defined by:

$$d' = \frac{\mu_{hit} - \mu_{miss}}{\sqrt{\frac{1}{2}(\sigma_{hit}^2 + \sigma_{miss}^2)}}$$

where μ denotes the mean and σ the standard deviation for hit and miss trials, respectively.

References

Alais D, Newell FN, Mamassian P. 2010. Multisensory processing in review: From physiology to behaviour. *Seeing Perceiving* **23**:3–38. doi:10.1163/187847510X488603

Arieli A, Sterkin A, Grinvald A, Aertsen A. 1996. Dynamics of ongoing activity: Explanation of the large variability in evoked cortical responses. *Science* **273**:1868–1871. doi:10.1126/science.273.5283.1868

Arnal LH, Poeppel D, Giraud AL. 2015. Temporal coding in the auditory cortex. *Handb Clin Neurol* **129**:85–98. doi:10.1016/B978-0-444-62630-1.00005-6

Bastos AM, Usrey WM, Adams RA, Mangun GR, Fries P, Friston KJ. 2012. Canonical microcircuits for predictive coding. *Neuron* **76**:695–711. doi:10.1016/j.neuron.2012.10.038

Bastos AM, Vezoli J, Bosman CA, Schoffelen J-M, Oostenveld R, Dowdall JR, De Weerd P, Kennedy H, Fries P. 2015. Visual areas exert feedforward and feedback influences through distinct frequency channels. *Neuron* **85**:390–401. doi:10.1016/j.neuron.2014.12.018

Bernasconi C, von Stein A, Chiang C, König P. 2000. Bi-directional interactions between visual areas in the awake behaving cat. *Neuroreport* **11**:689–692. doi:10.1097/00001756-200003200-00007

Bizley JK, Nodal FR, Bajo VM, Nelken I, King AJ. 2007. Physiological and anatomical evidence for multisensory interactions in auditory cortex. *Cereb Cortex* **17**:2172–2189. doi:10.1093/cercor/bhl128

Bizley, K, Bajo VM, Nodal FR, King AJ. 2015. Cortico-cortical connectivity within ferret auditory cortex. *J Comp Neurol* **523**: 2187–2210. doi:10.1002/cne.23784

Bockhorst T, Pieper F, Engler G, Stieglitz T, Galindo-Leon E, Engel AK. 2018. Synchrony surfacing: Epicortical recording of correlated action potentials. *Eur J Neurosci* **48**: 3583–3596. doi:10.1111/ejn.14167

Bosman CA, Schoffelen J-M, Brunet N, Oostenveld R, Bastos AM, Womelsdorf T, Rubehn B, Stieglitz T, De Weerd P, Fries P. 2012. Attentional stimulus selection through selective synchronization between monkey visual areas. *Neuron* **75**:875–888. doi:10.1016/j.neuron.2012.06.037

636 Brainard DH. 1997. The psychophysics toolbox. *Spat Vis* **10**:433–436.
637 doi:10.1163/156856897X00357
638 Brookes MJ, Hale JR, Zumer JM, Stevenson CM, Francis ST, Barnes GR, Owen JP, Morris PG,
639 Nagarajan SS. 2011a. Measuring functional connectivity using MEG: Methodology and
640 comparison with fcMRI. *NeuroImage* **56**:1082–1104. doi:10.1016/j.neuroimage.2011.02.054
641 Brookes MJ, Wood JR, Stevenson CM, Zumer JM, White TP, Liddle PF, Morris PG. 2011b. Changes
642 in brain network activity during working memory tasks: A magnetoencephalography study.
643 *NeuroImage* **55**:1804–1815. doi: 10.1016/j.neuroimage.2010.10.074
644 Busch NA, Dubois J, VanRullen R. 2009. The phase of ongoing EEG oscillations predicts visual
645 perception. *J Neurosci* **29**:7869–7876. doi:10.1523/JNEUROSCI.0113-09.2009
646 Buschman TJ, Miller EK. 2007. Top-down versus bottom-up control of attention in the prefrontal and
647 posterior parietal cortices. *Science* **315**:1860–1862. doi:10.1126/science.1138071
648 Buzsaki G. 2006. Rhythms of the brain. Oxford University Press.
649 Canolty RT, Knight RT. 2010. The functional role of cross-frequency coupling. *Trends Cogn Sci*
650 **14**:506–515. doi:10.1016/j.tics.2010.09.001
651 Coulter DA, Yue C, Ang CW, Weissinger F, Goldberg E, Hsu F-C, Carlson GC, Takano H. 2011.
652 Hippocampal microcircuit dynamics probed using optical imaging approaches. *J Physiol*
653 **589**:1893–1903. doi:10.1113/jphysiol.2010.202184
654 Crone NE, Sinai A, Korzeniewska A. 2006. High-frequency gamma oscillations and human brain
655 mapping with electrocorticography. *Prog Brain Res* **159**:275–295. doi:10.1016/S0079-
656 6123(06)59019-3
657 Donner TH, Siegel M, Fries P, Engel AK. 2009. Build-up of choice-predictive activity in human
658 motor cortex during perceptual decision making. *Curr Biol* **19**: 1581–1585.
659 doi:10.1016/j.cub.2009.07.066
660 Engel AK, Fries P. 2010. Beta-band oscillations--signalling the status quo? *Curr Opin Neurobiol*
661 **20**:156–165. doi:10.1016/j.conb.2010.02.015
662 Engel AK, Fries P, Singer W. 2001. Dynamic predictions: Oscillations and synchrony in top–down
663 processing. *Nat Rev Neurosci* **2**:704–716. doi:10.1038/35094565

664 Engel AK, Gerloff C, Hilgetag CC, Nolte G. 2013. Intrinsic coupling modes: Multiscale interactions
665 in ongoing brain activity. *Neuron* **80**:867–886. doi:10.1016/j.neuron.2013.09.038
666 Feldmeyer D, Brecht M, Helmchen F, Petersen CCH, Poulet JFA, Staiger JF, Luhmann HJ, Schwarz
667 C. 2013. Barrel cortex function. *Prog Neurobiol* **103**:3–27.
668 doi:10.1016/j.pneurobio.2012.11.002
669 Fell J, Axmacher N. 2011. The role of phase synchronization in memory processes. *Nat Rev Neurosci*
670 **12**:105–118. doi:10.1038/nrn2979
671 Fischer F, Pieper F, Galindo-Leon E, Engler G, Hilgetag CC, Engel AK. 2018. Intrinsic functional
672 connectivity resembles cortical architecture at various levels of isoflurane anesthesia. *Cereb*
673 *Cortex* **28**:2991–3003. doi:10.1093/cercor/bhy114
674 Fox KCR, Foster BL, Kucyi A, Daitch AL, Parvizi J. 2018. Intracranial electrophysiology of the
675 human default Network." *Trends Cogn Sci* **22**: 307–324. doi:10.1016/j.neuron.2007.08.023
676 Fries P, Neuenschwander S, Engel AK, Goebel R, Singer W. 2001. Rapid feature selective neuronal
677 synchronization through correlated latency shifting. *Nat Neurosci* **4**: 194–200.
678 doi:10.1038/84032
679 Fries P. 2005. A mechanism for cognitive dynamics: Neuronal communication through neuronal
680 coherence. *Trends Cogn Sci* **9**:474–480. doi:10.1016/j.tics.2005.08.011
681 Fukushima M, Chao ZC, Fujii N. 2015. Studying brain functions with mesoscopic measurements:
682 Advances in electrocorticography for non-human primates. *Curr Opin Neurobiol* **32**:124–131.
683 doi:10.1016/j.conb.2015.03.015
684 Galindo-Leon, E., Stitt, I., Pieper, F., Stieglitz, T., Engler, G., Engel, A.K., 2019. Context-specific
685 modulation of intrinsic coupling modes shapes multisensory processing. bioRxiv 509943.
686 doi:10.1101/509943
687 Ghazanfar AA, Chandrasekaran C, Logothetis NK. 2008. Interactions between the superior temporal
688 sulcus and auditory cortex mediate dynamic face/voice integration in rhesus monkeys. *J*
689 *Neurosci* **28**:4457–4469. doi:10.1523/JNEUROSCI.0541-08.2008

690 Giordano BL, Ince RAA, Gross J, Schyns PG, Panzeri S, Kayser C. 2017. Contributions of local
691 speech encoding and functional connectivity to audio-visual speech perception. *eLife* **6**.
692 doi:10.7554/eLife.24763
693 Giraud A-L, Poeppel D. 2012. Cortical oscillations and speech processing: Emerging computational
694 principles and operations. *Nat Neurosci* **15**:511–517. doi:10.1038/nn.3063
695 Green AM, Angelaki DE. 2010. Multisensory integration: Resolving sensory ambiguities to build
696 novel representations. *Curr Opin in Neurobiol* **20**:353–360. doi:10.1016/j.conb.2010.04.009
697 Gregoriou GG, Gotts SJ, Zhou H, Desimone R. 2009. High-frequency, long-range coupling between
698 prefrontal and visual cortex during attention. *Science* **324**:1207–1210.
699 doi:10.1126/science.1171402
700 Gross, J, Kujala J, Hamalainen M, Timmermann L, Schnitzler A, Salmelin R. 2001. Dynamic imaging
701 of coherent sources: Studying neural interactions in the human brain. *Proc Natl Acad Sci USA*
702 **98**: 694–699. doi:10.1073/pnas.98.2.694
703 Hanslmayr S, Aslan A, Staudigl T, Klimesch W, Herrmann CS, Bäuml K-H. 2007. Prestimulus
704 oscillations predict visual perception performance between and within subjects. *NeuroImage*
705 **37**:1465–1473. doi:10.1016/j.neuroimage.2007.07.011
706 Harris KD, Thiele A. 2011. Cortical state and attention. *Nat Rev Neurosci* **12**:509–523.
707 doi:10.1038/nrn3084
708 He BJ, Snyder AZ, Zempel JM, Smyth MD, Raichle ME. 2008. Electrophysiological correlates of the
709 brain's intrinsic large-scale functional architecture. *Proc Natl Acad Sci USA* **105**: 16039–
710 16044. doi:10.1101/pdb.top078147
711 Hipp JF, Engel AK, Siegel M. 2011. Oscillatory synchronization in large-scale cortical networks
712 predicts perception. *Neuron* **69**:387–396. doi:10.1016/j.neuron.2010.12.027
713 Hipp JF, Hawellek DJ, Corbetta M, Siegel M, Engel AK. 2012. Large-scale cortical correlation
714 structure of spontaneous oscillatory activity. *Nat Neurosci* **15**: 884–890. doi:10.1038/nn.3101
715 Hollensteiner KJ, Pieper F, Engler G, König P, Engel AK. 2015. Crossmodal integration improves
716 sensory detection thresholds in the ferret. *PLoS One* **10**:e0124952. doi:
717 10.1371/journal.pone.0124952

718 Hyvärinen A, Oja E. 2000. Independent component analysis: Algorithms and applications. *Neural*
719 *Netw* **13**:411–430. doi:10.1016/S0893-6080(00)00026-5
720 Jensen O, Mazaheri A. 2010. Shaping functional architecture by oscillatory alpha activity: Gating by
721 inhibition. *Front Hum Neurosci* **4**. doi:10.3389/fnhum.2010.00186
722 Kaernbach C. 1991. Simple adaptive testing with the weighted up-down method. *Perception &*
723 *Psychophysics* **49**:227–229. doi:10.3758/BF03214307
724 Kayser C, Petkov CI, Logothetis NK. 2008. Visual modulation of neurons in auditory cortex. *Cereb*
725 *Cortex* **18**:1560–1574. doi:10.1093/cercor/bhm187
726 Keil J, Müller N, Hartmann T, Weisz N. 2014. Prestimulus beta power and phase synchrony influence
727 the sound-induced flash illusion. *Cereb Cortex* **24**:1278–1288. doi:10.1093/cercor/bhs409
728 Keller CJ, Honey CJ, Mégevand P, Entz L, Ulbert I, Mehta AD. 2014. Mapping human brain networks
729 with cortico-cortical evoked potentials. *Philos Trans R Soc B Biol Sci* **369**:20130528.
730 doi:10.1098/rstb.2013.0528
731 Khodagholy D, Gelinas JN, Zhao Z, Yeh M, Long M, Greenlee JD, Doyle W, Devinsky O, Buzsáki G.
732 2016. Organic electronics for high-resolution electrocorticography of the human brain. Sci
733 Adv 2: e1601027. doi:10.1126/sciadv.1601027
734 Lachaux JP, Rodriguez E, Martinerie J, Varela FJ. 1999. Measuring phase synchrony in brain signals.
735 *Hum Brain Mapp* **8**:194–208. doi:10.1002/(SICI)1097-0193(1999)8:4<194::AID-
736 HBM4>3.0.CO;2-C
737 Lakatos P, Chen C-M, O'Connell MN, Mills A, Schroeder CE. 2007. Neuronal oscillations and
738 multisensory interaction in primary auditory cortex. *Neuron* **53**:279–292.
739 doi:10.1016/j.neuron.2006.12.011
740 Lewis C, Bosman C, Fries P. 2015. Recording of brain activity across spatial scales. *Curr Opin*
741 *Neurobiol* **32**:68–77. doi:10.1016/j.conb.2014.12.007
742 Liebe S, Hoerzer GM, Logothetis NK, Rainer G. 2012. Theta coupling between V4 and prefrontal
743 cortex predicts visual short-term memory performance. *Nature Neuroscience* **15**:456–462.
744 doi:10.1038/nn.3038

745 Maier JX, Chandrasekaran C, Ghazanfar AA. 2008. Integration of bimodal looming signals through
746 neuronal coherence in the temporal lobe. *Curr Biol* **18**:963–968.
747 doi:10.1016/j.cub.2008.05.043
748 Michalareas G, Vezoli J, van Pelt S, Schoffelen J-M, Kennedy H, Fries P. 2016. Alpha-beta and
749 gamma rhythms subserve feedback and feedforward influences among human visual cortical
750 areas. *Neuron* **89**:384–397. doi:10.1016/j.neuron.2015.12.018
751 Miller EK, Buschman TJ. 2013. Cortical circuits for the control of attention. *Curr Opin Neurobiol*
752 **23**:216–222. doi:10.1016/j.conb.2012.11.011
753 Munk MH, Roelfsema PR, König P, Engel AK, Singer W. 1996. Role of reticular activation in the
754 modulation of intracortical synchronization. *Science* **272**: 271–274.
755 doi:10.1126/science.272.5259.271
756 Nodal FR, Bajo VM, Parsons CH, Schnupp JW, King AJ. 2008. Sound localization behavior in ferrets:
757 Comparison of acoustic orientation and approach-to-target responses. *Neuroscience* **154**:397–
758 408. doi:10.1016/j.neuroscience.2007.12.022
759 Nolte G, Bai O, Wheaton L, Mari Z, Vorbach S, Hallett M. 2004. Identifying true brain interaction
760 from EEG data using the imaginary part of coherency. *Clin Neurophysiol* **115**: 2292–2307.
761 doi:10.1016/j.clinph.2004.04.029
762 O'Neill GC, Tewarie PK, Colclough GL, Gascoyne LE, Hunt BAE, Morris PG, Woolrich MW,
763 Brookes MJ. 2017. Measurement of dynamic task related functional networks using MEG.
764 *NeuroImage* **146**:667–678. doi:10.1016/j.neuroimage.2016.08.061
765 Ploner M, Sorg C, Gross J. 2017. Brain rhythms of pain. *Trends Cogn Sci* **21**: 100–110.
766 doi:10.1016/j.tics.2016.12.001
767 Raichle ME. 2010. Two views of brain function. *Trends Cogn Sci* **14**:180–190.
768 doi:10.1016/j.tics.2010.01.008
769 Roelfsema PR, Engel AK, König P, Singer W. 1997. Visuomotor integration is associated with zero
770 time-lag synchronization among cortical areas. *Nature* **385**:157-161. doi:10.1038/385157a0
771 Rose M, Büchel C. 2005. Neural coupling binds visual tokens to moving stimuli. *J Neurosci* **25**:
772 10101–10104. doi:10.1523/JNEUROSCI.2998-05.2005

773 Rubehn B, Bosman C, Oostenveld R, Fries P, Stieglitz T. 2009. A MEMS-based flexible multichannel
774 ECoG-electrode array. *J Neural Eng* **6**:036003. doi:10.1088/1741-2560/6/3/036003
775 Saalmann YB, Pinsk MA, Wang L, Li X, Kastner S. 2012. The pulvinar regulates information
776 transmission between cortical areas based on attention demands. *Science* **337**:753–756.
777 doi:10.1126/science.1223082
778 Salazar RF, Dotson NM, Bressler SL, Gray CM. 2012. Content-specific fronto-parietal
779 synchronization during visual working memory. *Science* **338**:1097–1100.
780 doi:10.1126/science.1224000
781 Senkowski D, Schneider TR, Foxe JJ, Engel AK. 2008. Crossmodal binding through neural
782 coherence: implications for multisensory processing. *Trends Neurosci* **31**:401–409.
783 doi:10.1016/j.tins.2008.05.002
784 Shadlen MN, Britten KH, Newsome WT, Movshon JA. 1996. A computational analysis of the
785 relationship between neuronal and behavioral responses to visual motion. *J Neurosci* **16**:1486–
786 1510. doi:10.1523/JNEUROSCI.16-04-01486.1996
787 Siegel M, Donner TH, Engel AK. 2012. Spectral fingerprints of large-scale neuronal interactions. *Nat*
788 *Rev Neurosci* **13**:121–134. doi:10.1038/nrn3137
789 Siegel M, Donner TH, Oostenveld R, Fries P, Engel AK. 2008. Neuronal synchronization along the
790 dorsal visual pathway reflects the focus of spatial attention. *Neuron* **60**: 709-719.
791 doi:10.1016/j.neuron.2008.09.010
792 Singer W, Gray CM. 1995. Visual feature integration and the temporal correlation hypothesis. *Annu*
793 *Rev Neurosci* **18**:555–586. doi:10.1146/annurev.ne.18.030195.003011
794 Singer W. 1999. Neuronal synchrony: A versatile code for the definition of relations?" *Neuron* **24**: 49–
795 65, 111. doi:10.1016/S0896-6273(00)80821-1
796 Stein BE, Meredith A. 1993. The merging of the senses. Cambridge, Mass.: MIT Press.
797 Steriade M, Contreras D, Amzica F, Timofeev I. 1996. Synchronization of fast (30-40 Hz)
798 spontaneous oscillations in intrathalamic and thalamocortical networks. *J Neurosci* **16**:2788–
799 2808. doi:10.1523/JNEUROSCI.16-08-02788.1996

800 Steriade M, McCormick DA, Sejnowski TJ (1993) Thalamocortical oscillations in the sleeping and
801 aroused brain. *Science* **262**: 679–685. doi:10.1126/science.8235588
802 Stitt I, Hollensteiner KJ, Galindo-Leon E, Pieper F, Fiedler E, Stieglitz T, Engler G, Nolte G, Engel
803 AK. 2017. Dynamic reconfiguration of cortical functional connectivity across brain states. *Sci*
804 *Rep* **7**:8797. doi:10.1038/s41598-017-08050-6
805 Supp GG, Siegel M, Hipp JF, Engel AK. 2011. Cortical hypersynchrony predicts breakdown of
806 sensory processing during loss of consciousness." *Curr Biol* **21**: 1988–1993.
807 doi:10.1016/j.cub.2011.10.017
808 Talsma D, Senkowski D, Soto-Faraco S, Woldorff MG. 2010. The multifaceted interplay between
809 attention and multisensory integration. *Trends Cogn Sci* **14**:400–410.
810 doi:10.1016/j.tics.2010.06.008
811 Toda H, Kawasaki K, Sato S, Horie M, Nakahara K, Bepari AK, Sawahata H, Suzuki T, Okado H,
812 Takebayashi H, Hasegawa I. 2018. Locally induced neuronal synchrony precisely propagates
813 to specific cortical areas without rhythm distortion. *Sci Rep* **8**: 7678. doi:10.1038/s41598-018-
814 26054-8
815 van Atteveldt N, Murray MM, Thut G, Schroeder CE. 2014. Multisensory integration: Flexible use of
816 general operations. *Neuron* **81**:1240–1253. doi:10.1016/j.neuron.2014.02.044
817 van den Brink RL, Nieuwenhuis S, Donner TH. 2018. Amplification and suppression of distinct
818 brainwide activity patterns by catecholamines. *J Neurosci* **38**: 7476–7491.
819 doi:10.1523/JNEUROSCI.0514-18.2018
820 Varela F, Lachaux JP, Rodriguez E, Martinerie J. 2001. The brainweb: Phase synchronization and
821 large-scale integration. *Nat Rev Neurosci* **2**:229–239. doi:10.1038/35067550
822 Wang P, Goeschl F, Friese U, Koenig P, Engel AK. 2018. Long-range functional coupling predicts
823 performance: Oscillatory EEG networks in multisensory processing. *bioRxiv* 014423. doi:
824 10.1101/014423
825 Womelsdorf T, Fries P, Mitra PP, Desimone R. 2006. Gamma-band synchronization in visual cortex
826 predicts speed of change detection. *Nature* **439**: 733–736. doi:10.1038/nature04258

827 Womelsdorf T, Fries P. 2007. The role of neuronal synchronization in selective attention. *Curr Opin*
828 *Neurobiol* **17**:154–160. doi:10.1016/j.conb.2007.02.002
829 Womelsdorf T, Schoffelen J-M, Oostenveld R, Singer W, Desimone R, Engel AK, Fries P. 2007.
830 Modulation of neuronal interactions through neuronal synchronization. *Science* **316**: 1609–
831 1612. doi:10.1126/science.1139597
832 Zohary E, Shadlen MN, Newsome WT. 1994. Correlated neuronal discharge rate and its implications
833 for psychophysical performance. *Nature* **370**:140. doi:10.1038/370140a0

Acknowledgements

We would like to thank Dorrit Bystron for her assistance throughout experiments. This research was supported by funding from the DFG (SFB 936/A2, SPP 1665/EN533/13-1, SPP 2041/EN533/15-1, A.K.E.; SFB936/Z3, G.N.).

Competing Interests

They are no competing interests.

Author Contributions

K.J.H, F.P. and A.K.E. conceived and designed experiments. G.E. wrote animal ethics permission. K.J.H and F.P. surgically implanted arrays. K.J.H. performed experiments. K.J.H., F.P., E.G.L. and G.N. provided analyzing tools. K.J.H. analyzed data. K.J.H. and A.K.E. wrote the paper. All authors edited and approved the manuscript.

Figure Legends

Figure 1. Experimental setup and lateralized detection task. (A) Schematic of the experimental setup in a top view: a) LED-screen, b) speakers, c) three light-barrier-waterspout combinations (left, center, right; the red dot indicates a broken light-beam), d) pedestal, e) semi-circular acrylic tube accommodating the animal's body. (B) Sequence of events in a single trial: (I) inter-trial window, (II) baseline window, (III) stimulus window, and (IV) response window. The three circles below each frame represent the state of the light-barriers (white = unbroken, red = broken). The center of the screen displays a static circular random noise pattern.

Figure 2. Trial selection for electrophysiological analysis and corresponding RTs. (A) Example data for task performance from one ferret. The plot shows for the uni- and bimodal audio condition. Stimulus response function fitted to performance data for the eight different stimulus intensities for the unimodal auditory condition (A) and the condition where the variable auditory stimulus was accompanied by a visual stimulus of constant contrast (Av). The dot diameter indicates the number of trials at a given stimulus intensity. The green ellipse indicates the stimulus intensity range around 75% performance from which trials were selected for subsequent analysis. The unmasked parts of the graphs indicate the range of the actually tested stimulus amplitudes. (B) Data from the same animal as shown in A for the unimodal visual condition (V) and the condition where the variable visual stimulus was accompanied by an auditory stimulus of constant intensity (Va). (C) Grand average of reaction times (RT; sec.±standard deviation) for the four different conditions for the selected trials. Asterisks indicate significant differences between modalities or pooled data from bimodal (Va and Av) and unimodal (A and V) stimulus pairs (brackets).

Figure 3. Spectral power analysis of pooled hit and miss trials. (A) Trial timeline with analysis windows (baseline, stimulus and response onset, respectively); insets show screen frames and sensory stimulation. (B) Time-frequency representation of power in the three analysis time windows, expressed as change relative to baseline before trial onset for all hit and miss trials. The vertical line

represents trial, stimulus and response onset, respectively. (C) Grand average power spectra for all hit (green) and miss (red) trials±standard error of the mean (SEM). For the baseline window absolute power is shown. Note that for the windows around stimulus and response onset, the spectral change relative to the baseline window is displayed. Asterisks indicate significant differences between hits and misses within the specified frequency band (FDR corrected). Labels in C indicate theta, alpha, beta, gamma and high-gamma band, respectively.

Figure 4. Grand average of functional connectivity for hit and miss trials. (A) Grand average phase locking value (PLV) for all hit (green) and miss (red) trials for the analysis time windows (baseline, stimulus- and response-onset). (B) Differences between hits and misses for the three analysis windows and changes of PLV around stimulus- and response-onset, expressed as changes relative to the baseline window. Asterisks indicate significant differences between hits and misses within the specified frequency band (FDR corrected). Labels in A denote theta, alpha, beta, gamma and high-gamma band, respectively.

Figure 5. Matrices of functional connectivity across anatomical areas. Cells show population average phase locking values (PLV) for the different frequency bands, expressed as d' for hits vs. misses, for all analysis time windows. Abbreviations: S2, secondary somatosensory cortex; PPr/c, rostral/caudal posterior parietal cortex; 17, 18, 19, 20, 21, early and higher-order visual cortex; SSY, suprasylvian field; A1, primary auditory cortex; AAF, anterior auditory field; ADF, anterior dorsal field; PPF, posterior pseudosylvian field; PSF, posterior suprasylvian field.

Figure 6. Comparison of long-range (between-systems) and short-range (within-system) functional connectivity. (Left) Cortical regions were grouped into visual (magenta), parietal (blue), or auditory (orange) systems. PLV was averaged for all pairs of regions that were located within the same system (grey arrows) and pairs between systems (red arrows). Subsequently, d' was calculated for hit and miss trial PLVs. (Right) Differences of between-region and within-region PLV (d') are plotted as a function of carrier frequencies. Large values indicate higher between-system PLV during

hit compare to miss trials. Symbols indicate significant differences between baseline and stimulus onset (*), baseline and response onset (o), and stimulus onset to response onset (+), respectively.

Figure 7. ECoG recordings from the ferret brain. (A). Lateral view of the left hemisphere. Lines mark sulci on the posterior part. (B) Functional and anatomical organization of the posterior part of the ferret brain; adopted from Bizley et al. (2007). (C) Schematic of the implanted ECoG (contact spacing: 1.5mm; ø: 250µm). (D) In-situ picture of the ECoG array over the left posterior hemisphere during implantation. Abbreviations: LS, lateral sulcus; SSS, suprasylvian sulcus; other abbreviations as in Fig. 5.

Tables

Table 1. Statistics for frequency resolved power analysis for hit and miss trials. The table shows *p*-values for all *t*-tests within frequency bands, trial outcome, and across all time points of interest; *italics* indicate significant comparisons ($p<0.001$; FDR corrected).

Frequency	Theta	Alpha	Beta	Gamma	High-Gamma
	Baseline vs. stimulus onset window				
Hit vs. hit	0.22	0.26	0.44	*>0.001*	0.053
Miss vs. miss	0.23	0.54	0.99	*>0.001*	*>0.001*
	Stimulus onset vs. response onset window				
Hit vs. hit	0.03	0.18	0.08	*>0.001*	*>0.001*
Miss vs. miss	0.21	0.62	0.53	0.08	*>0.001*
	Response onset window vs. baseline				
Hit vs. hit	0.10	0.46	0.98	0.01	*>0.001*
Miss vs. miss	0.25	0.58	0.79	*>0.001*	*>0.001*

Table 2. Statistics for frequency resolved functional connectivity analysis for all time points of interest for hit and miss trials. The table shows *p*-values for all *t*-tests within frequency bands, trial outcome and across all time points of interest; *italics* indicate significant contrasts (FDR corrected).

Frequency	Theta	Alpha	Beta	Gamma	High-Gamma
	Baseline vs. stimulus onset window				
Hit vs. hit	0.12	*<0.001*	*<0.001*	*<0.001*	*<0.001*
Miss vs. miss	0.75	*<0.001*	*<0.001*	*<0.001*	*<0.001*
	Stimulus onset vs. response onset window				
Hit vs. hit	0.03	*<0.001*	0.36	*<0.001*	*<0.001*
Miss vs. miss	0.79	0.07	0.67	0.17	*<0.001*
	Response onset window vs. baseline				
Hit vs. hit	*<0.001*	0.02	0.003	*<0.001*	*<0.001*
Miss vs. miss	0.84	*<0.001*	*<0.001*	*<0.001*	*<0.001*

Supplements

Supplementary Figure 1. Spectral power for uni- and bimodal stimulation conditions. Grand average power spectra for baseline, stimulus- and response-onset for all hit trials (green), all miss trials (red) and for the hit trials of each stimulus condition (Av: blue; Va: yellow; A: orange; V: purple). For the baseline window absolute power is shown. Note that for the windows centered around stimulus and response onset, the spectral change relative to the baseline window is displayed. For ANOVA results, see Supplementary Table 1.

Supplementary Figure 2. Frequency specific power topographies for all analysis time windows. Topographic representation of power for all frequency bands and analysis time windows, expressed as d' for the difference between hits and misses. High values indicate dominance during hit compare to miss trials. Negative values indicate increased power during the miss compare to hit trials. Abbreviations: LS, lateral sulcus; SSS, suprasylvian sulcus.

Supplementary Figure 3. Grand average functional connectivity for uni- and bimodal stimulation conditions. Grand average phase locking value (PLV) for all analysis time windows (baseline, stimulus and response onset) for all hit trials (green), all miss trials (red) and for the hit trials of each stimulus condition (Av: blue; Va: yellow; A: orange; V: purple).

Supplementary Figure 4. Within- and between system functional connectivity for all frequencies and analysis time windows. Cortical regions were grouped into visual (magenta), parietal (blue), or auditory (orange) systems. PLV was averaged for all pairs of regions that were located within the same system (grey arrows) and pairs between systems (red arrows). Bar plots display the sensitivity index (d') for difference between hit and miss trial PLV for the theta, alpha, beta, gamma, high-gamma frequency bands, as well as for broadband (BB) data averaged across all frequency bands. Panels show data for within system PLV (left) and between system PLV (right) for all analysis time

windows. Lines between bars indicate significant differences. For ANOVA results, see Supplementary Table 5.

Supplementary Figure 5. Modality specific comparison of long-range (between-systems) and short-range (within-system) functional connectivity. (Top) Cortical regions were grouped into visual (magenta), parietal (blue), or auditory (orange) systems. PLV was averaged for all pairs of regions that were located within the same system (grey arrows) and pairs between systems (red arrows). Subsequently, d' was calculated for hit and miss trial PLVs. (Bottom) Plots shows the differences of between-region and within-region PLV (d') as a function of carrier frequencies for each stimulation condition (Top left: A; top right: V; bottom left: Av; bottom right: Va). Large values indicate higher between-system PLV during hit compare to miss trials. Symbols indicate significant differences between baseline and stimulus onset (*), baseline and response onset (o), and stimulus onset to response onset (+), respectively. For modality specific ANOVA and post hoc *t*-test results see Supplementary Tables 6-9.

963 **Supplementary Table 1.** One-way ANOVA results between the four conditions (Av, Va, A and V) as
964 main factor for the data shown in Supplementary Figure 1.

Frequency	Theta	Alpha	Beta	Gamma	High-Gamma
Time					
Baseline	$F(3, 44) = 0.02$, $p>0.05$	$F(3, 76) = 0.03$, $p>0.05$	$F(3, 60) = 0.01$, $p>0.05$	$F(3, 412) = 0.02$, $p>0.05$	$F(3, 652) = 0.09$, $p>0.05$
Stimulus onset	$F(3, 44) = 0.03$, $p>0.05$	$F(3, 76) = 0.01$, $p>0.05$	$F(3, 60) = 0$, $p>0.05$	$F(3, 412) = 0.4$, $p>0.05$	$F(3, 652) = 0.06$, $p>0.05$
Response onset	$F(3, 44) = 0.02$, $p>0.05$	$F(3, 76) = 0.03$, $p>0.05$	$F(3, 60) = 0.02$, $p>0.05$	$F(3, 412) = 0.05$, $p>0.05$	$F(3, 652) = 0.07$, $p>0.05$

965

966 **Supplementary Table 2.** *p*-values of the post hoc *t*-test results for data shown in Supplementary
967 Figure 3 for the baseline analysis window; *italics* indicate significant contrasts (Bonferroni corrected).

Frequency	Theta	Alpha	Beta	Gamma	High-Gamma
A → V	>0.05	*0.004*	*0.035*	*<0.001*	*<0.001*
A → Av	>0.05	>0.05	>0.05	>0.05	>0.05
A → Va	>0.05	>0.05	>0.05	*<0.001*	*<0.001*
V → Av	>0.05	>0.05	>0.05	*<0.001*	*<0.001*
V →Va	>0.05	>0.05	>0.05	*0.038*	*0.003*
Av → Va	>0.05	>0.05	>0.05	*<0.001*	*<0.001*

968

969 **Supplementary Table 3.** *p*-values of the post hoc *t*-test results for data shown in Supplementary
970 Figure 3 for the stimulus onset analysis window; *italics* indicate significant contrasts (Bonferroni
971 corrected).

Frequency	Theta	Alpha	Beta	Gamma	High-Gamma
A → V	>0.05	*0.022*	*0.025*	*<0.001*	*<0.001*
A → Av	>0.05	>0.05	>0.05	>0.05	>0.05
A → Va	>0.05	>0.05	>0.05	*<0.001*	*<0.001*
V → Av	>0.05	>0.05	>0.05	*<0.001*	*<0.001*
V →Va	>0.05	>0.05	>0.05	>0.05	*0.002*
Av → Va	>0.05	>0.05	>0.05	*<0.001*	*<0.001*

972

Supplementary Table 4. *p*-values of the post hoc *t*-test results for data shown in Supplementary Figure 3 for the response onset analysis window; *italics* indicate significant contrasts (Bonferroni corrected).

Frequency	Theta	Alpha	Beta	Gamma	High-Gamma
A → V	>0.05	*0.035*	*0.02*	*<0.001*	*<0.001*
A → Av	>0.05	>0.05	>0.05	>0.05	>0.05
A → Va	>0.05	>0.05	>0.05	*<0.001*	*<0.001*
V → Av	>0.05	>0.05	>0.05	*<0.001*	*<0.001*
V →Va	>0.05	>0.05	>0.05	>0.05	*0.005*
Av → Va	>0.05	>0.05	>0.05	*0.002*	*<0.001*

Supplementary Table 5. Two-way ANOVA results with System (within auditory; within visual; within parietal; between visual and auditory; between visual and parietal: between auditory and parietal) and Time (Baseline, stimulus and response onset) as main factors for the data shown in Supplementary Figure 4.

Frequency	Theta	Alpha	Beta	Gamma	High-Gamma	Broadband
ANOVA						
System	$F(5, 375) = 17.69$, p<0.001	$F(5, 375) = 30.55$, p<0.001	$F(5, 375) = 17.31$, p<0.001	$F(5, 375) = 18.9$, p<0.001	$F(5, 375) = 15.45$, p<0.001	$F(5, 375) = 18.85$, p<0.001
Time	$F(2, 375) = 12.17$, p<0.001	$F(2, 375) = 8.33$, p<0.001	$F(2, 375) = 5.4$, p=0.005	$F(2, 375) = 7.15$, p<0.001	$F(2, 375) = 6.79$, p=0.001	$F(2, 375) = 12.23$, p<0.001
Interaction	$F(10, 375) = 0.88$, p>0.05	$F(10, 375) = 0.55$, p>0.05	$F(10, 375) = 0.6$, p>0.05	$F(10, 375) = 0.35$, p>0.05	$F(10, 375) = 0.44$, p>0.05	$F(10, 375) = 0.51$, p>0.05

Supplementary Table 6. ANOVA and post hoc *t*-test (*p*-values) results for data shown in Supplementary Figure 5 for the auditory modality; *italics* indicate significant contrasts (Bonferroni corrected). Abbreviations: BL = Baseline; SO = Stimulus-onset; RO = Response-onset.

Frequency	Theta	Alpha	Beta	Gamma	High-Gamma
ANOVA	$F(2, 6) = 0.23$, p>0.05	$F(2, 12) = 7.32$, p=0.008	$F(2, 9) = 8.03$, p=0.01	$F(2, 75) = 7.45$, p=0.001	$F(2, 120) = 5.01$, p=0.008
Post hoc *t*-test					
BL → SO	>0.05	0.04	0.01	*0.004*	0.01
SO → RO	>0.05	>0.05	>0.05	*0.004*	>0.05
BL → RO	>0.05	0.01	>0.05	>0.05	>0.05

Supplementary Table 7. ANOVA and post hoc *t*-test (*p*-values) results for data shown in Supplementary Figure 5 for the visual modality; *italics* indicate significant contrasts (Bonferroni corrected). Abbreviations: BL = Baseline; SO = Stimulus-onset; RO = Response-onset.

Frequency	Theta	Alpha	Beta	Gamma	High-Gamma
ANOVA	$F(2, 6) = 4.21$, $p>0.05$	$F(2, 12) = 8.53$, $p=0.005$	$F(2, 9) = 5.33$, $p=0.03$	$F(2, 75) = 10.62$, $p<0.001$	$F(2, 120) = 9.63$, $p<0.001$
Post hoc *t*-test					
BL → SO	>0.05	>0.05	>0.05	*0.001*	*0.001*
SO → RO	>0.05	>0.05	>0.05	>0.05	*0.002*
BL → RO	>0.05	*0.004*	0.04	>0.05	>0.05

Supplementary Table 8. ANOVA and post hoc *t*-test (*p*-values) results for data shown in Supplementary Figure 5 for the auditory stimulation accompanied by a constant visual stimulus (Av); *italics* indicate significant contrasts (Bonferroni corrected). Abbreviations: BL = Baseline; SO = Stimulus-onset; RO = Response-onset.

Frequency	Theta	Alpha	Beta	Gamma	High-Gamma
ANOVA	$F(2, 6) = 1.65$, $p>0.05$	$F(2, 12) = 12.14$, $p=0.001$	$F(2, 9) = 5.25$, $p=0.031$	$F(2, 75) = 10.37$, $p<0.001$	$F(2, 120) = 17.96$, $p<0.001$
Post hoc *t*-test					
BL → SO	>0.05	0.02	0.04	*0.001*	*<0.001*
SO → RO	>0.05	>0.05	>0.05	>0.05	*0.006*
BL → RO	>0.05	*0.001*	>0.05	0.01	0.02

Supplementary Table 9. ANOVA and post hoc *t*-test (*p*-values) results for the data shown in Supplementary Figure 5 for the visual stimulation accompanied by a constant auditory stimulus (Va); *italics* indicate significant contrasts (Bonferroni corrected). *Abbreviations:* BL = Baseline; SO = Stimulus-onset; RO = Response-onset.

Frequency	Theta	Alpha	Beta	Gamma	High-Gamma
ANOVA	$F(2, 6) = 5.09$, $p>0.05$	$F(2, 12) = 6.66$, $p=0.011$	$F(2, 9) = 4.07$, $p>0.05$	$F(2, 75) = 5.88$, $p=0.004$	$F(2, 120) = 11.12$, $p<0.001$
Post hoc *t*-test					
BL → SO	>0.05	>0.05	>0.05	0.04	*<0.001*
SO → RO	>0.05	>0.05	>0.05	>0.05	0.03
BL → RO	>0.05	0.01	>0.05	>0.05	>0.05

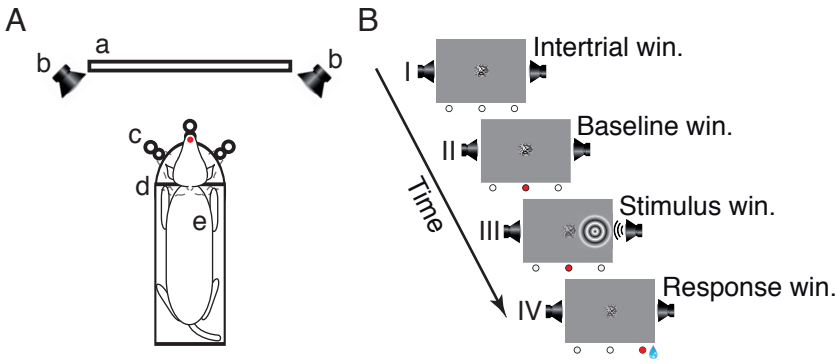

Figure 1

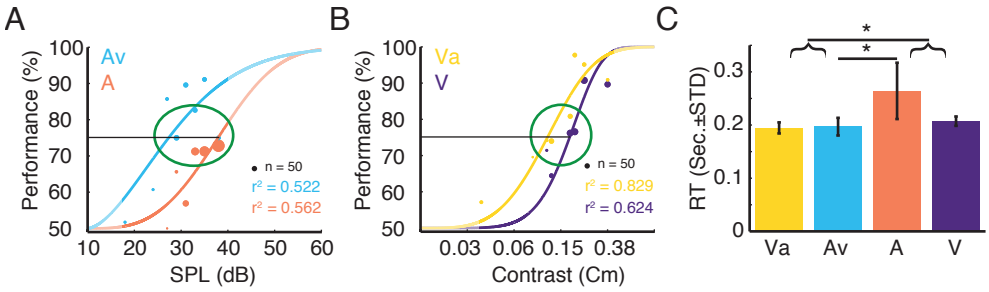

Figure 2

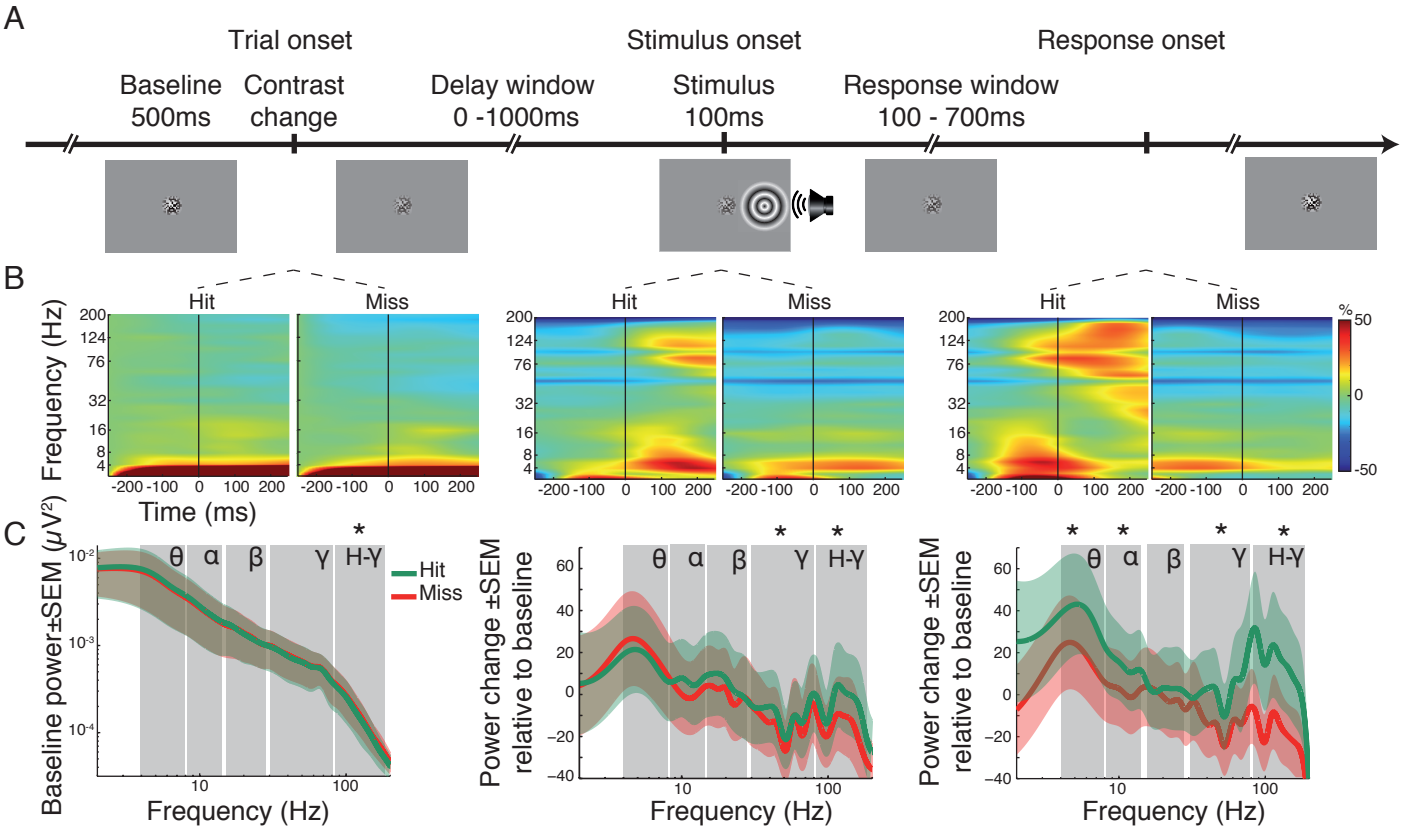

Figure 3

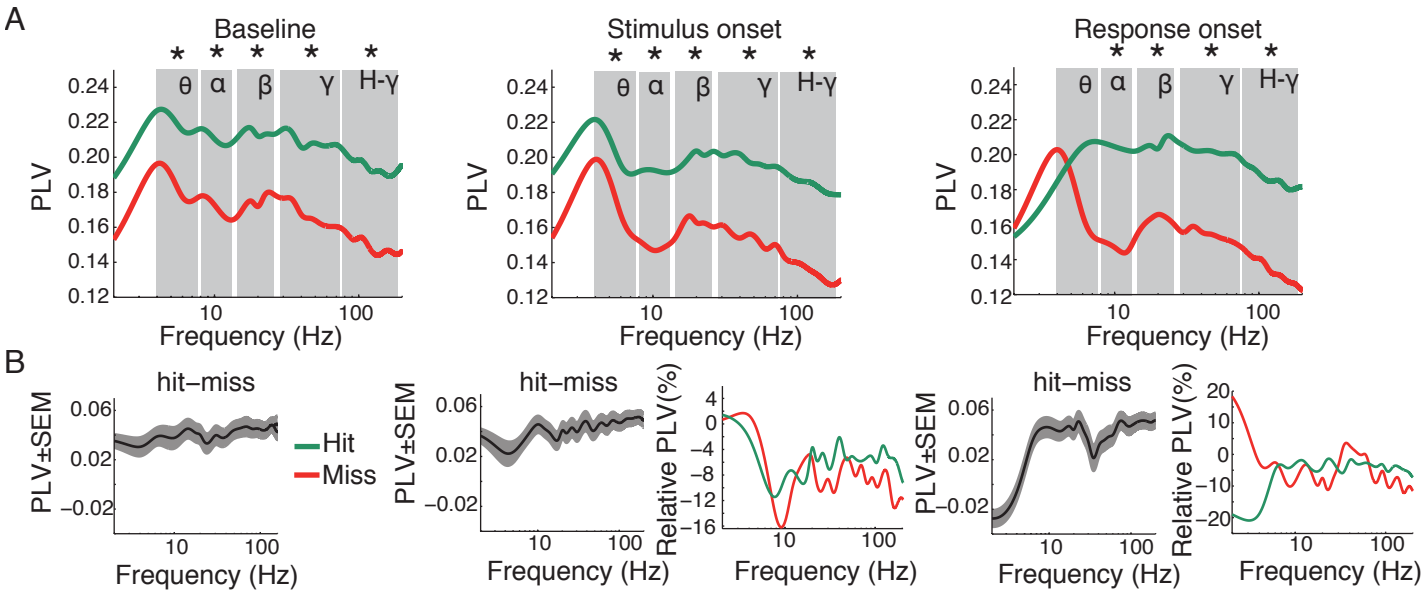

Figure 4

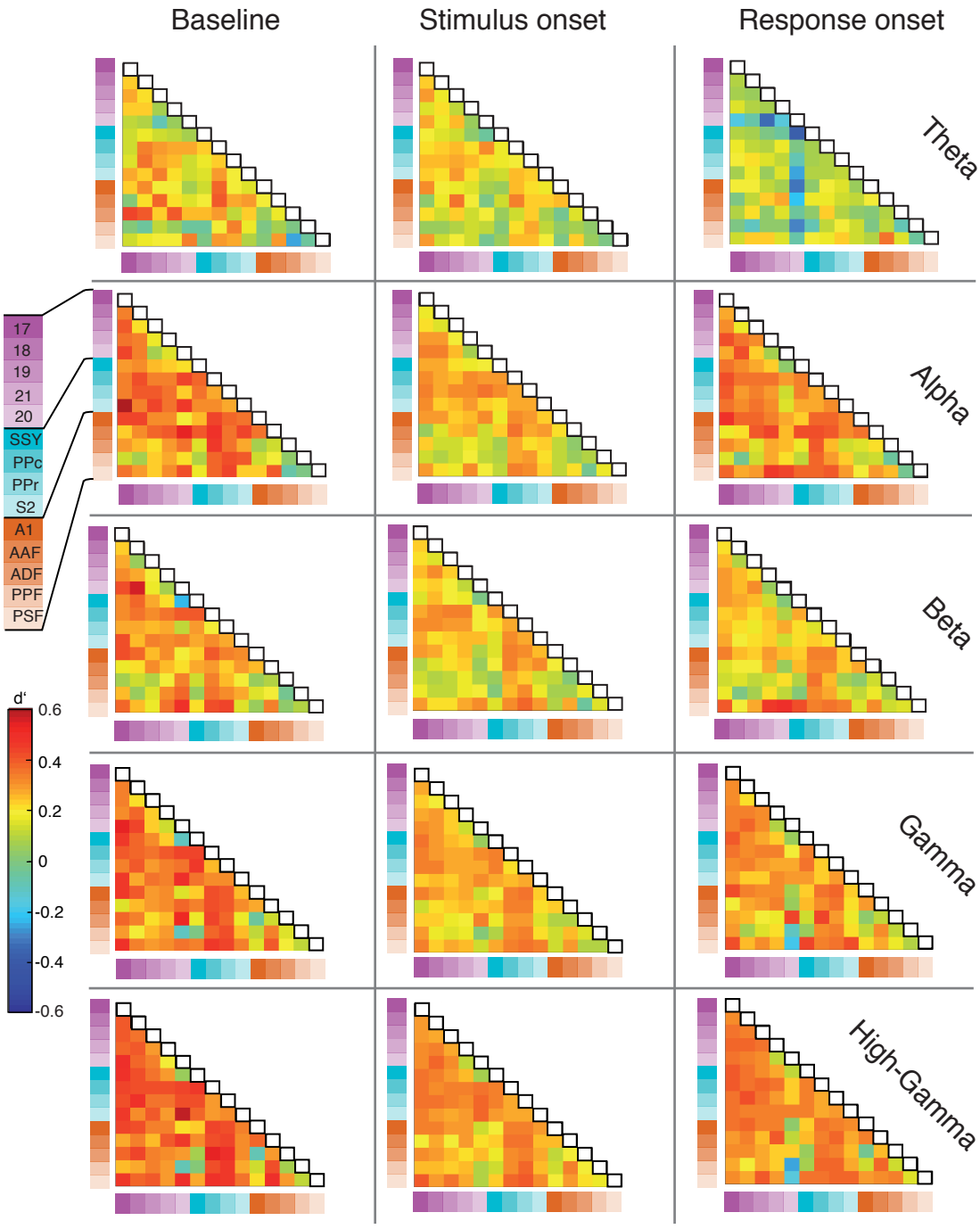

Figure 5

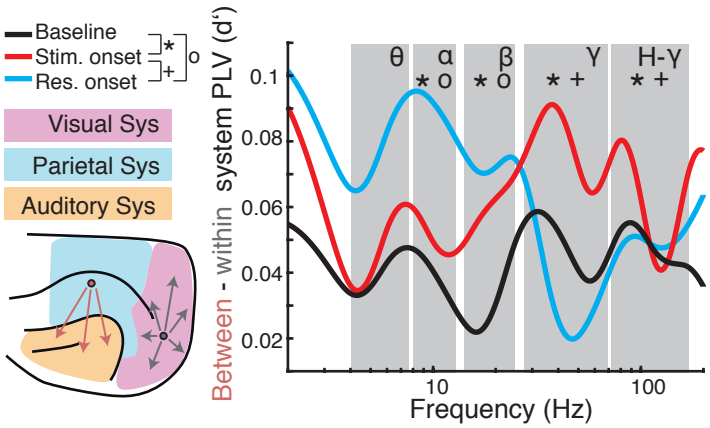

Figure 6

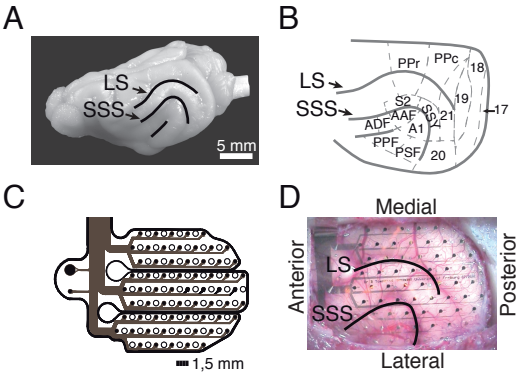

Figure 7

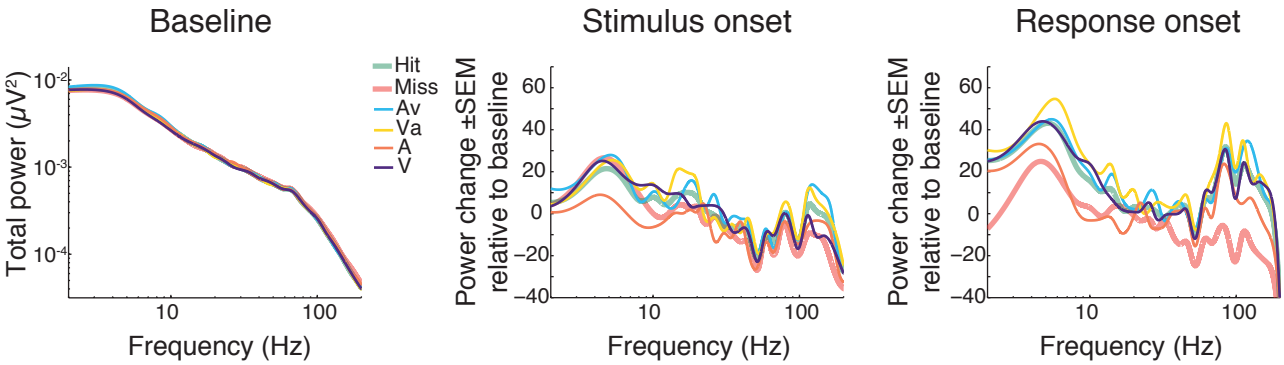

Supplementary Figure 1

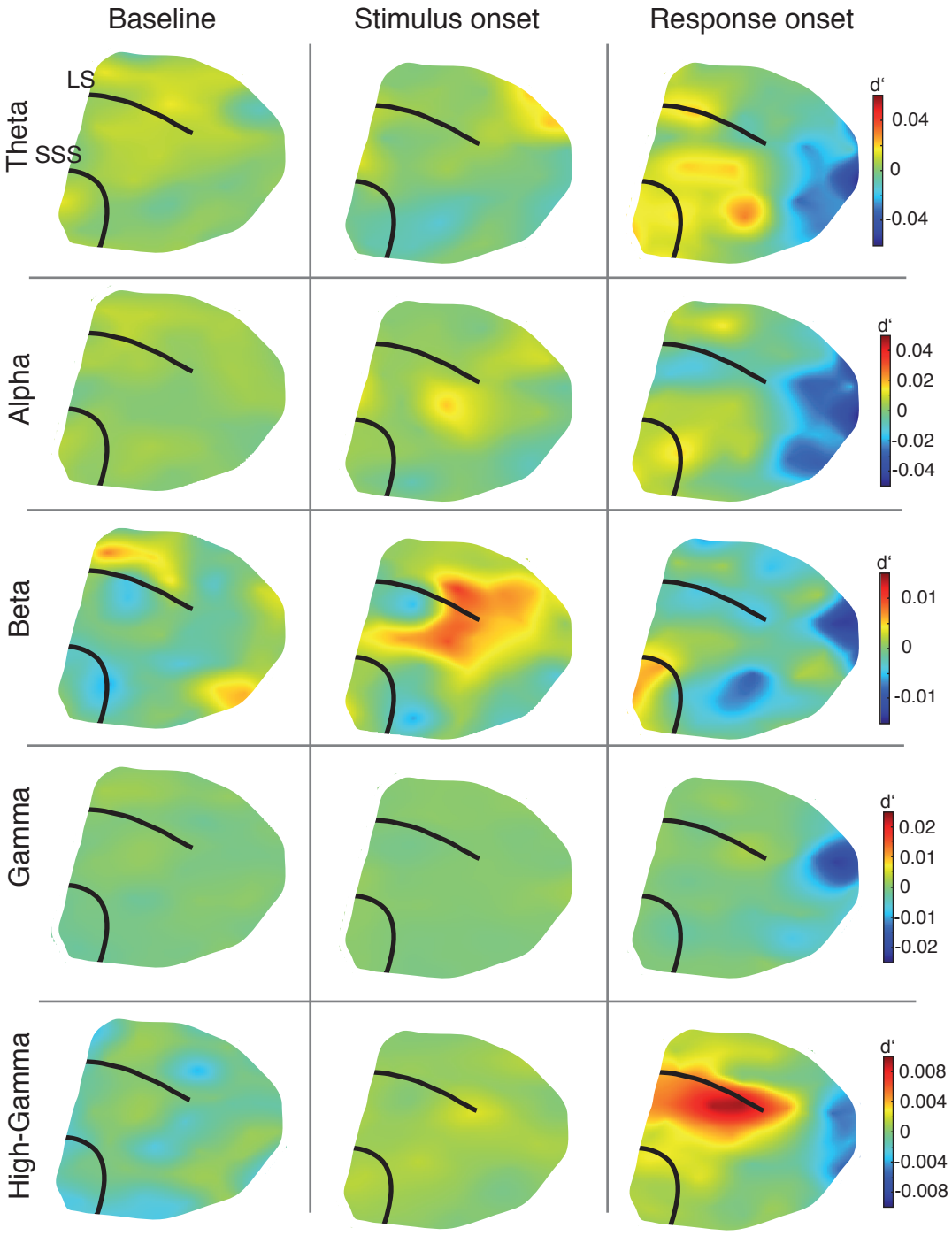

Supplementary Figure 2

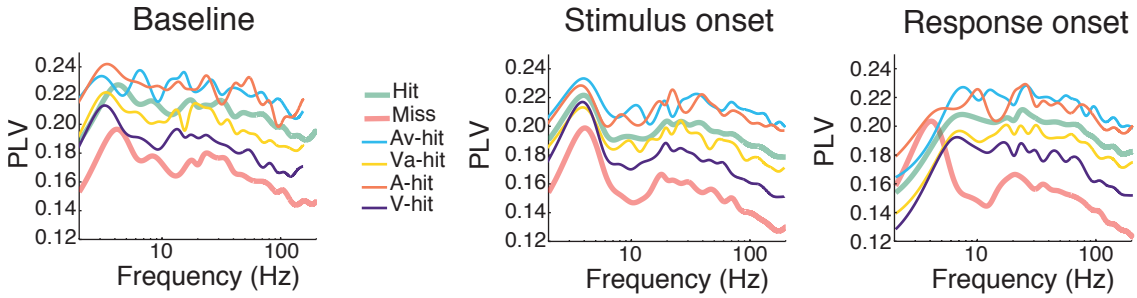

Supplementary Figure 3

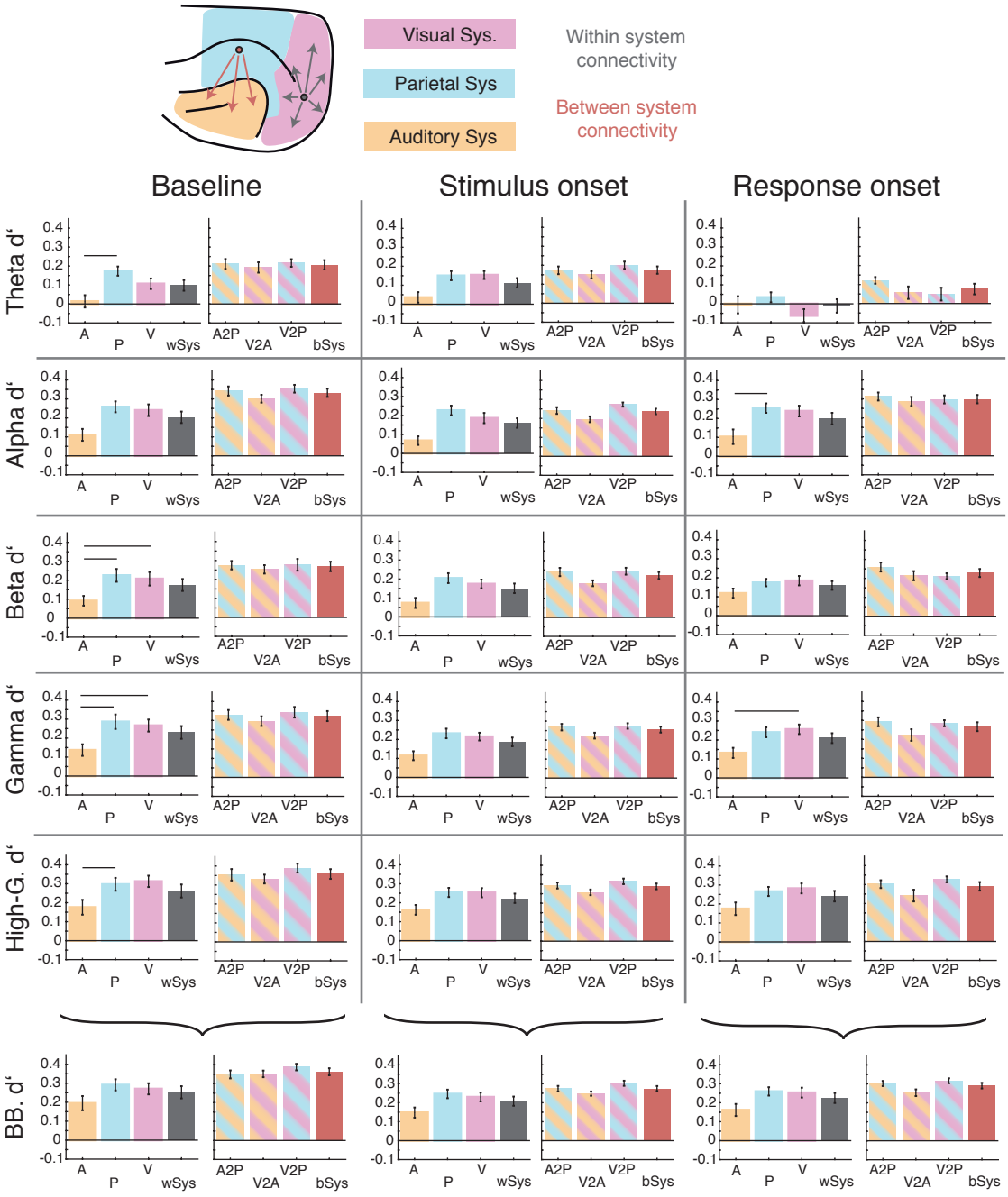

Supplementary Figure 4

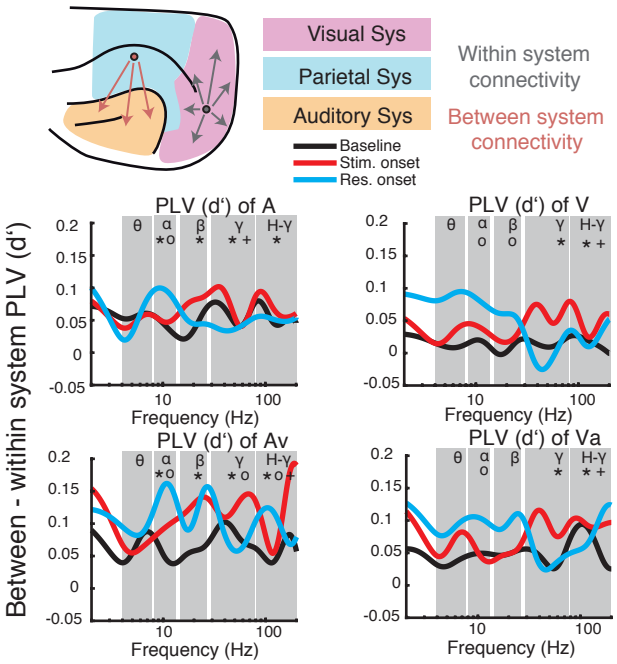

Supplementary Figure 5